Available online at www.sciencedirect.com

ScienceDirect

Underground Space 27 (2026) 386–405

www.keaipublishing.com/undsp

Research Paper

Incomplete soil arching effect and responses of existing tunnels induced by undercrossing super-large-diameter shield tunneling in soft strata

Yuyang Cao [a,b], Xiongyao Xie [a,b,*], Kun Zeng [a,b], Yangbin Zhang [a,b], Haiyang Tian [c], Jian Yao [d], Junliang Zong [c]

[a] *Department of Geotechnical Engineering, College of Civil Engineering, Tongji University, Shanghai 200092, China*
[b] *Key Laboratory of Geotechnical and Underground Engineering of Ministry of Education, Tongji University, Shanghai 200092, China*
[c] *Shanghai Huangpu Infrastructure Investment Construction and Development Co., Ltd., Shanghai 200080, China*
[d] *Shanghai Urban Construction Design and Research Institute (Group) Co., Ltd., Shanghai 200125, China*

Received 5 September 2024; received in revised form 10 April 2025; accepted 22 April 2025
Available online 17 February 2026

Abstract

Super-large-diameter shield tunneling inevitably induces deformations in the surrounding soil and nearby existing tunnels due to ground-tunnel interactions. This study developed and validated a numerical model to simulate these interactions in typical soft soil strata in Shanghai, with a focus on stress and displacement responses during the undercrossing of an existing tunnel by a new super-large-diameter shield tunnel. The study identified an incomplete soil arching (ISA) effect and proposed methods to delineate the ISA, loosened, and compaction zones, categorizing the influenced areas into reinforced, stable, and safe zones. Parametric analyses examined the influence of tunnel spacing (S) and volume loss ratio (V) on ground deformation, loosened zone height, and existing tunnel deformation. Results indicate that greater volume loss ratios and smaller tunnel spacings amplify ground settlement, while the loosened zone height is affected by both the volume loss ratio and the stratigraphic boundary. Among the considered scenarios, a volume loss ratio of 0.2% minimizes the loosened zone height across various spacings. Changes in the convergence of the existing tunnel occur in two phases, characterized by rapid changes (S/D of 0.1–0.3, where D is the diameter of the newly constructed tunnel) and gradual changes (S/D of 0.3–0.7). To mitigate adverse effects on the ground and the existing tunnel, it is recommended to maintain the volume loss ratio below 0.2% and the tunnel spacing over 0.3D. Additionally, reinforcing the loosened zone is advised to enhance the stability of the existing tunnel.

Keywords: Super-large-diameter shield; Undercrossing; Numerical simulation; Ground responses; Existing tunnel deformation; Incomplete soil arching (ISA)

1 Introduction

Urbanization has exacerbated traffic congestion, necessitating the construction of underground metro tunnels, which often intersect existing tunnels at small spacings. Shield tunneling alters the stress and displacement fields in surrounding strata (Khandouzi & Khosravi, 2023; Soga et al., 2017), inducing additional loads and deformations in adjacent existing tunnels (Chen et al., 2018;). Under challenging conditions, such as narrow tunnel spacings, high volume loss, or large-diameter tunneling, existing tunnels may risk severe damage, including cracks, seepage, and misalignment (Huang et al., 2018; Li & Yuan, 2012; Wu et al., 2020), compromising their structural integrity. Additionally, undercrossing tunneling can deform the ground surface, disrupting the stability of surface buildings (Xie et al., 2016). A comprehensive understanding of shield

* Corresponding author at: Department of Geotechnical Engineering, College of Civil Engineering, Tongji University, Shanghai 200092, China.
E-mail address: xiexiongyao@tongji.edu.cn (X. Xie).
Peer review under the responsibility of Tongji University

https://doi.org/10.1016/j.undsp.2025.04.013

excavation's impact on the ground and existing tunnel is crucial for risk mitigation and ensuring structural safety.

The impacts of undercrossing tunneling on the ground and existing tunnels are typically assessed through four methods: empirical/theoretical analyses, model tests, field measurements, and numerical simulations. Empirical studies mainly predict the ground surface settlement (Fargnoli et al., 2013; Peck, 1969), while theoretical approaches, such as Winkler, Pasternak, or Kerr foundation models, analyze the existing tunnel deformation during shield tunneling (Ding et al., 2023; Gan et al., 2022; Klar et al., 2005). Centrifuge (Fang et al., 2022; Li et al., 2014; Ng et al., 2015) and model tests (Lin et al., 2021, 2022; Yang et al., 2017) investigate deformation and stress responses of existing tunnels, including interactions among the new tunnel, surrounding strata, and existing tunnels (Weng et al., 2022). Field measurements provide reliable data on the responses of the ground and existing tunnels to validate protective measures (Chen et al., 2018; Cooper et al., 2002; Jin et al., 2018). Numerical simulations are widely used for analyzing stress and deformation under various scenarios (Avgerinos et al., 2017; Do et al., 2014; Jin et al., 2019; Lai et al., 2020; Lin et al., 2019a; Liu et al., 2022). For example, Avgerinos et al. (2017) simulated deformation and stress responses of existing tunnels induced by orthogonal undercrossing tunneling, and Jin et al. (2019) further examined the influence of tunnel spacing and positioning. Liu et al. (2022) developed a calculation model using equivalent-layer and mirror methods to simulate vertical deformation of existing tunnels due to orthogonal undercrossing, and further performed a series of orthogonal tests to assess parameter sensitivity.

Although extensive research has focused on the deformation of the ground and existing tunnels, the underlying mechanisms remain underexplored due to insufficient analysis of stress redistribution in the surrounding strata. Numerical models have revealed stress redistribution and soil arching evolution induced by shield tunneling. Lin et al. (2019b) studied the formation of the tunneling-induced soil arching and loosened zones, and Song et al. (2023) further proposed a method to determine the soil arching and loosened zones in clayey soil layers. Chen et al. (2013) and Lee et al. (2006) developed criteria for delineating soil arching boundaries. Nevertheless, these studies did not consider the presence of existing tunnels. Lin et al. (2019a) investigated the existing tunnel and ground responses during shield tunneling and identified soil stress redistribution at the crown and bottom of the existing tunnel, attributing this to the soil arching effect. However, they only provided a schematic of the soil arching zone without quantitatively defining its boundaries.

Furthermore, most studies have focused on existing tunnels undercrossed by small-diameter tunnels, leaving the impacts of undercrossing by super-large-diameter tunnels underexplored. Tunnels with diameters under 10 m are classified as small or medium, those between 10 and 15 m as large, and those over 15 m as super-large-diameter tunnels (Zhu et al., 2022). The rising demand for urban underground expressways has increased instances of super-large-diameter shield tunnels undercrossing existing small-diameter tunnels at close spacings. These super-large-diameter tunnels, due to their greater unloading capacity (Zhu et al., 2022), may induce different effects on the ground and existing tunnels compared to smaller-diameter tunnels. Consequently, studying these impacts and developing effective protection measures are essential.

Therefore, the effects of super-large-diameter shield tunnels undercrossing existing tunnels at close spacings remain insufficiently studied. Specifically, the evolution of stress and displacement in the strata, especially near existing tunnels, remains inadequately understood. To address these gaps, this study develops and validates a numerical model to analyze stress and displacement responses in soft strata induced by the undercrossing of an existing tunnel by a super-large-diameter shield tunnel. It further reveals incomplete soil arching effects, proposes a reinforced zone, and optimizes tunnel spacing and volume loss ratio through parametric analyses.

2 Case background and verification of the numerical model

2.1 Overview of the case background

In this study, the case of Shanghai North-Cross Tunnel (NT) undercrossing Metro Line 7 was selected for model validation. As shown in Fig. 1(a), Metro Line 7, operational since 2009, was constructed using the earth pressure balance (EPB) shield method. NT sequentially underpassed the upline (UL) and downline (DL) of Metro Line 7, with the crossing node located 17.5 m from Changshou Road station. Metro Line 7 is buried at a depth of 16.51 m, with outer and inner tunnel diameters of 6.2 and 5.5 m, respectively. Each segmental ring is 1.2 m long, and the UL–DL axis spacing is 15.2 m. NT was constructed using a Φ15 560 mm slurry pressure balance (SPB) shield machine and is buried at a depth of 29.87 m, with outer and inner diameters of 15.0 and 13.7 m, respectively. It intersects Metro Line 7 at approximately 89° (an almost orthogonal crossing), with a minimum vertical spacing of 7.16 m. As shown in Fig. 1(b), Metro Line 7 mainly lies in silty clay, while NT passes primarily through silty sand and silty fine sand. According to Shanghai local regulation DG/TJ 08—2434—2023 (Shanghai Shentong Metro Group Co., Ltd. et al., 2023), the allowable deformation for shield tunnels is limited to 10 mm. To comply with this criterion, grouting protection was implemented to effectively control the deformation of Metro Line 7. During the undercrossing process of NT, vertical deformations of the existing Metro Line 7 tunnels were automatically monitored, providing a basis for model validation.

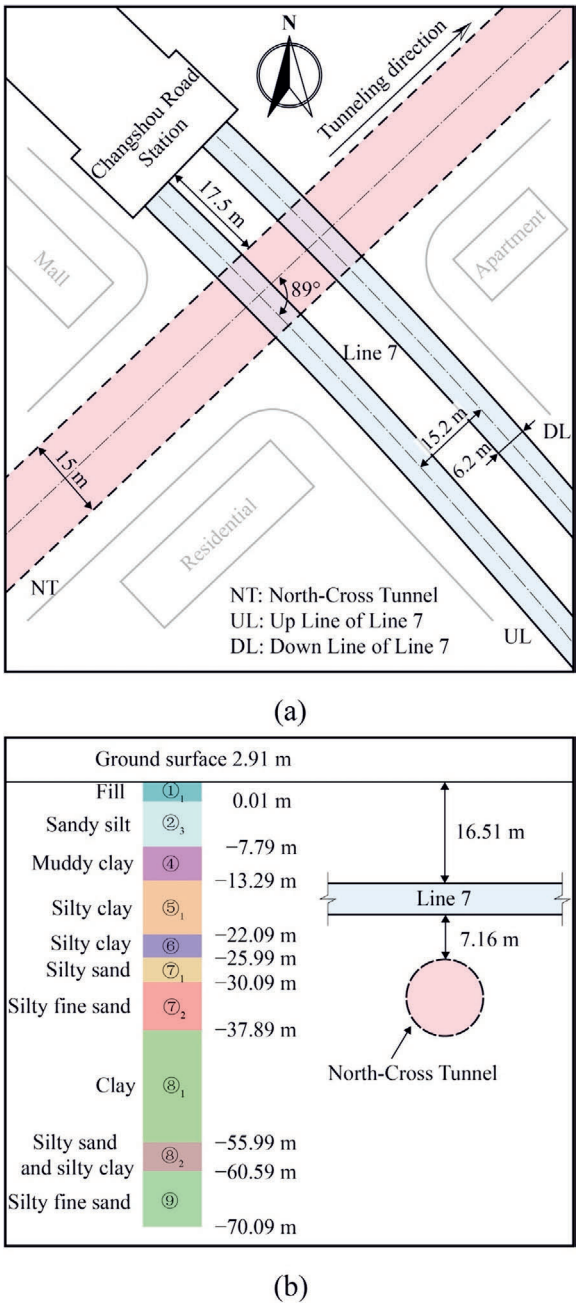

Fig. 1. Schematic of the North-Cross Tunnel undercrossing the existing Metro Line 7. (a) Plan view, and (b) representative soil profile.

2.2 Three-dimensional numerical simulation of the case

2.2.1 Numerical model

The numerical model (Fig. 2(a)) measures 145 m × 100 m × 100 m, with roller boundaries laterally, a free upper boundary representing the ground surface, and a fixed bottom boundary. Given the proximity of the crossing node to Changshou Road station, the station was incorporated to account for its potential impacts. Monitoring data indicated minimal displacement at the station during NT undercrossing. Thus, the station was modeled as a high-stiffness linear elastic body to simplify calculations while providing structural constraint for Line 7. Following trial calculations, the rigid block's weight was set at 18.4 kN/m^3, matching the weight of the surrounding soil to prevent excessive settlement or flotation. Figure 2(b) illustrates the rigid block model with dimensions 45 m × 28 m × 11 m.

2.2.2 Constitutive model and material parameters

In the numerical simulation, Metro Line 7 and the SPB shield were modeled using plate elements, while NT, the rigid block, and surrounding soils were simulated by tetrahedral elements. The tunnel lining, SPB shield, and rigid block were treated as isotropic, linearly elastic materials. To account for stiffness reduction due to circumferential and longitudinal joints, effective rigidity ratios of 0.7 and 0.1 were applied in the circumferential (Chen et al., 2016) and longitudinal directions (Lin et al., 2019a), respectively, with corresponding elastic moduli of 24.15 and 3.45 GPa. Interfacial elements were incorporated to simulate soil-structure interactions, with interface strength calibrated to 0.67, given the silty clay layer. The material parameters are summarized in Table 1.

The soil behavior was modeled using the Hardening Soil model with Small Strain Stiffness (HSS), an enhancement of the Hardening Soil (HS) model (Benz, 2006). The HSS model includes the shear and compression hardening features of the HS model, while additionally incorporating nonlinear stiffness behavior at small strains, providing a more accurate simulation of soil response to shield tunneling. The parameters for the HSS model, shown in Table 2, were based on geological data and empirical parameters for typical soil layers in Shanghai from Wang et al. (2013). These were validated by fitting computed results with field data (see Section 2.3).

2.2.3 Simulation of the construction process

The simulation process comprised three stages:

(1) Station construction (rigid block): Soil parameters were replaced with those of the rigid block to model station construction.
(2) Excavation of Metro Line 7: The excavation process was simulated after the station construction. Upon completion of stages (1) and (2), all displacements in soil and structures were reset to zero to provide a baseline for subsequent excavation activities.
(3) Excavation of the NT: NT excavation was modeled using construction parameters from the project report. Specifically, the face pressure at the top of the tunnel was set at 480 kPa with a gradient of 18 kPa/m, while the grouting pressure at the top was 600 kPa with a gradient of 20 kPa/m. The length of the SPB shield was established at 12 m, with the front 10 m programmed to contract linearly at an increment of −0.03%/m (C_{inc}), and the rear 2 m set for a uniform contraction of 0.3% (C_{ref}) to simulate volume loss. To efficiently simulate the process of

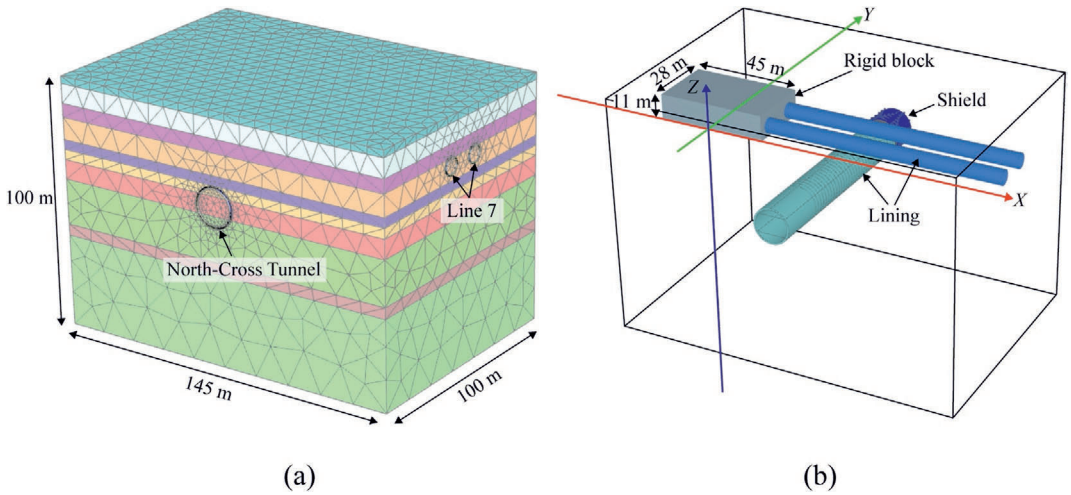

Fig. 2. Numerical model setup. (a) Geometry of the meshed numerical model, and (b) details of the new tunnel, existing tunnels, and rigid block.

Table 1
Material parameters of structures in the numerical model.

Material	Thickness t (m)	Volumetric weight γ (kN·m^{-3})	Young's modulus E (MPa)	Poisson's ratio v
Lining of NT	0.65	25	3.65×10^4	0.2
Lining of Line 7	0.35	25	3.45×10^4	0.2
SPB shield	0.28	120	2.30×10^5	0
Rigid block	11	18.4	3.00×10^4	0.2

Table 2
Parameters of the HSS model.

Soil layers	γ (kN·m^{-3})	c' (kPa)	φ' (°)	ψ (°)	G_0^{ref} (MPa)	$\gamma_{0.7}$ (10^{-4})	p^{ref} (kPa)	m	v_{ur}	R_f
①$_1$	18.5	4.35	32.30	0	65	2	100	0.8	0.2	0.9
②$_3$	18.2	4.35	32.30		77	2	100	0.8	0.2	0.9
④	16.6	11.20	26.00		58	2	100	0.8	0.2	0.6
⑤$_1$	18.1	8.40	27.03		66	2	100	0.8	0.2	0.9
⑥	19.6	20.00	36.77		141	2	100	0.8	0.2	0.9
⑦$_1$	18.6	4.69	29.44		177	2	100	0.5	0.2	0.9
⑦$_2$	18.7	4.69	29.44		177	2	100	0.5	0.2	0.9
⑧$_{1\text{-}1}$	18.4	6.10	30.00		95	2	100	0.8	0.2	0.9
⑧$_2$	18.5	3.04	34.00		124	2	100	0.8	0.2	0.9
⑨	18.7	6.60	38.00	8	190	2	100	0.5	0.2	0.9

Note: γ is the soil unit weight; c' is the effective cohesion; φ' is the effective friction angle; ψ is the dilatancy angle; G_0^{ref} is the reference shear modulus at exceedingly small strains ($\varepsilon < 10^{-6}$); $\gamma_{0.7}$ is the shear strain at which $G_s = 0.772G_0$; p^{ref} is the reference stress; m is the power that controls the stress dependency of stiffness; v_{ur} is the Poisson's ratio of unloading/reloading; R_f is the failure ratio.

shield tunneling, the SPB shield began its operation 30 m away from the UL and continued until the shield tail was 30 m past the DL. The tunneling was executed in a total of 37 steps, with each excavation step covering 2 m (the width of 1 ring).

2.3 Verification of the numerical model

The settlements of Line 7 were measured as the shield tunneling machine approached the position indicated in Fig. 3(a), where the excavation of NT was in progress. At this time point, the shield was about to traverse the intersection zone. Figure 3(b) and (c) compares the calculated and measured settlements for the UL and DL, respectively, using the Metro Line 7 station intersection point as the reference point. The calculated UL settlement trough closely matches the measured data (Fig. 3(b)), and the DL remains uplift within a 100 m range from the reference point, consistent with the trend observed in the measured data (Fig. 3(c)). The discrepancies between simulation and field data primarily result from the simplifications of

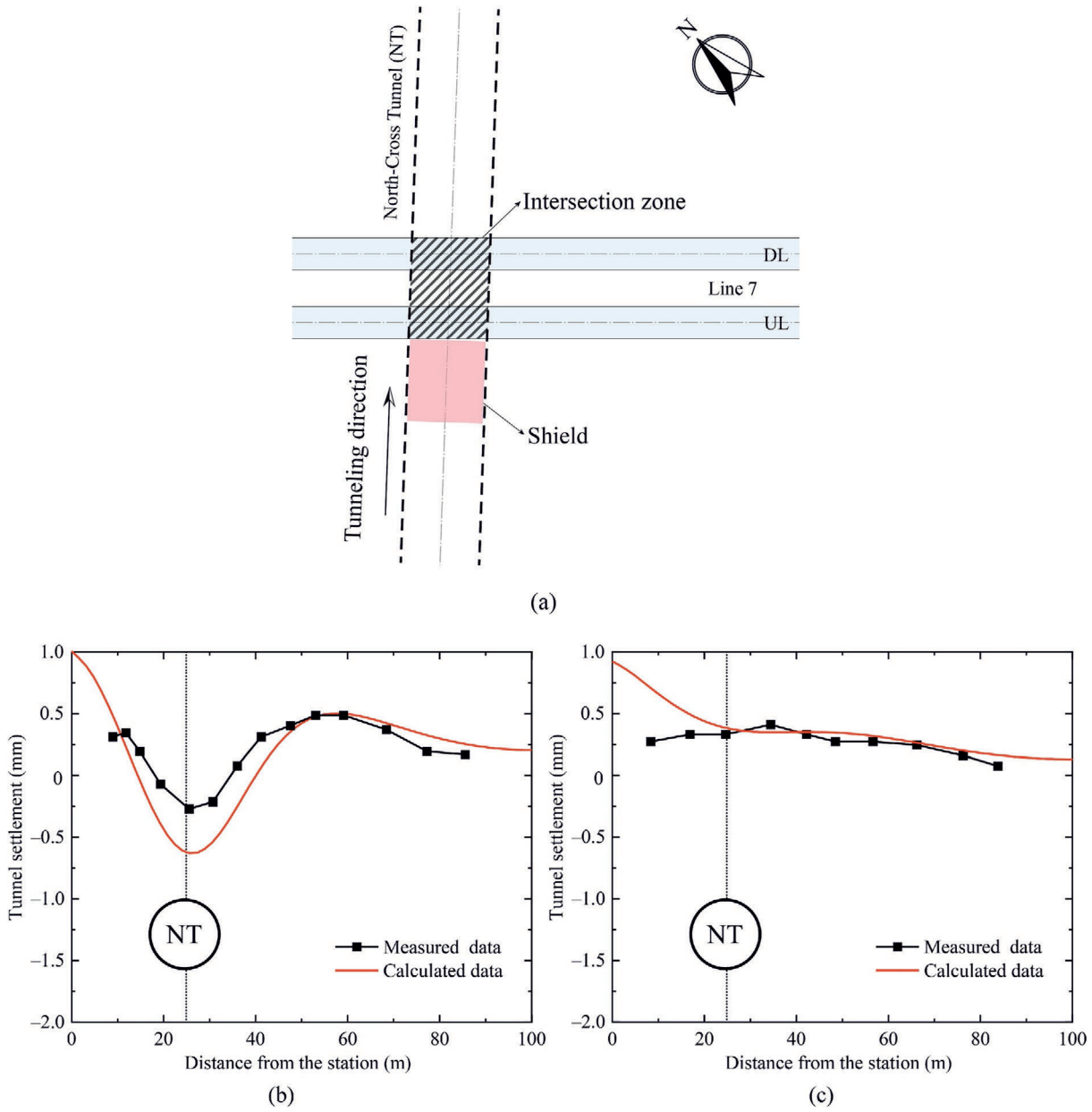

Fig. 3. Comparison between calculated and measured tunnel settlements for Line 7. (a) Schematic of the scenario when the shield is about to traverse the intersection zone, (b) UL, and (c) DL.

the metro station in our numerical model. In practice, the station construction implemented reinforcement measures, including (1) grouting, (2) the installation of diaphragm walls for foundation reinforcement, and (3) the use of steel supports and piles for structural reinforcement (Guo & Jiang, 2022; Qiu et al., 2023). These measures significantly enhanced the capability of the station to constrain the settlement of Line 7. However, in our model, the station is simplified as a rigid block, leading to a relatively weaker constraining effect than in reality. Consequently, the calculated settlements or heaves slightly exceed the measured values in Fig. 3(b) and (c). Despite these simplifications, the numerical results align well with the overall trends and magnitudes of field data, validating the reliability of our method and parameters for subsequent research.

3 Shield tunneling simulation of super-large-diameter tunnel

3.1 Numerical model

To analyze stress and displacement fields in strata affected by shield tunneling near existing tunnels, we developed a numerical model simulating a super-large-diameter shield tunnel orthogonally undercrossing a smaller existing one, a scenario particularly relevant given the frequent use of orthogonal undercrossing in new tunnel constructions near existing ones for safety reasons. The model reflects the complex soft strata of Shanghai, ensuring practical applicability. To minimize boundary effects, the model dimensions are set to 200 m in length and 110 m in width and height. The existing tunnel has a diameter (d) of

6.2 m, whereas the new tunnel features a larger diameter (D) of 15 m. This study systematically investigates various configurations with different spacings and volume loss ratios, as detailed in Section 3.2. The existing small-diameter tunnel is fixed at a burial depth of 16.5 m in all cases. The material parameters align with those in Section 2. The numerical model excludes the station area, as it is not the primary focus of our current study. Tunneling initiates at $Y = 0$ m and advances in 2 m increments over 55 steps.

As shown in Fig. 4, the left half of the model is dedicated to presenting the measurement section and points for monitoring stress and deformation. Positioned at $Y =$ 55 m, this section is crucial for analyzing ground responses during shield tunneling. Measurements are taken at seven strategic points along the tunnel centerline within this section: P_1 at the ground surface; P_2 and P_3 at the crown and bottom of the existing tunnel; and P_6 and P_7 at the crown and bottom of the new tunnel. The distances between P_3 and P_4, and between P_5 and P_6, are set at $0.1D$ and $0.07D$, respectively, facilitating detailed analysis of the spatial variations of stress and deformation.

Additionally, section I-I' focuses on the deformation of the existing tunnel. The vertical distance between the crown of the new tunnel and the bottom of the existing tunnel defines the tunnel spacing (S), which is a key parameter in assessing tunnel interactions.

3.2 Cases for analysis

To examine the influence of tunnel spacing and volume loss ratio on ground and existing tunnels, we developed 28 numerical models (Table 3). As shield tunneling projects increasingly navigate near existing tunnels with small spacings, some encounter vertical spacings as small as 1.5 m (Liu et al., 2022). Accordingly, this study sets the minimum tunnel spacing at 1.5 m ($0.1D$). Furthermore, based on statistical data from large-diameter shield construction in soft soil (Wu & Zhu, 2018), the volume loss ratio in this study is defined within a range of 0.2% to 1.4%.

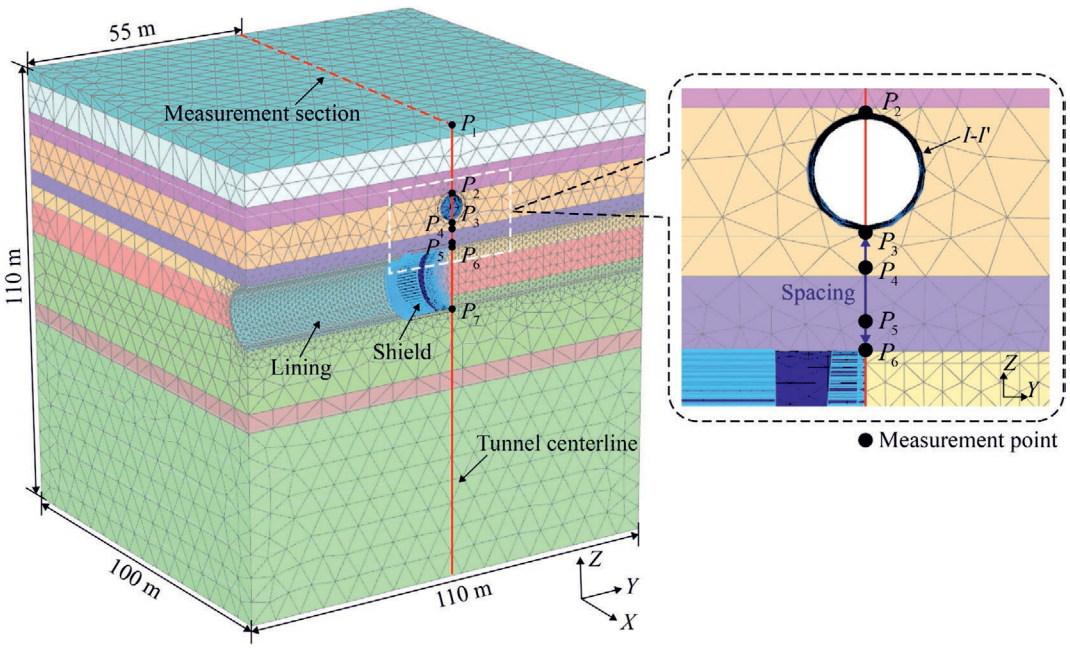

Fig. 4. Left half of the numerical model, showing positions of the measurement section and points.

Table 3
Cases for analysis.

Case group	S	Case ($V = 0.2\%$)	Case ($V = 0.6\%$)	Case ($V = 1.0\%$)	Case ($V = 1.4\%$)
1	$0.1D$	1-1	1-2	1-3	1-4
2	$0.2D$	2-1	2-2	2-3	2-4
3	$0.3D$	3-1	3-2	3-3	3-4
4	$0.4D$	4-1	4-2	4-3	4-4
5	$0.5D$	5-1	5-2	5-3	5-4
6	$0.6D$	6-1	6-2	6-3	6-4
7	$0.7D$	7-1	7-2	7-3	7-4

Note: S and V represent the tunnel spacing and volume loss ratio, respectively.

In the following section, Case 4-2, characterized by moderate spacing and volume loss ratio, is analyzed in detail. Figure 5(a) and (b) illustrates the measurement lines and points for Case group 4 ($S = 0.4D$). In Fig. 5(c), L denotes the distance between the tunnel face and the measurement section. A negative L indicates that the tunnel face is approaching the measurement section, while a positive L signifies that it has passed through.

4 Ground responses

Case 4-2 investigated the evolution of deformation and stress fields in the strata during shield tunneling near an existing tunnel, revealing the phenomenon of incomplete soil arching (ISA). The analysis focused on soil weakening and damage mechanisms induced by tunneling, providing essential insights for the protection of existing tunnels. Fur-

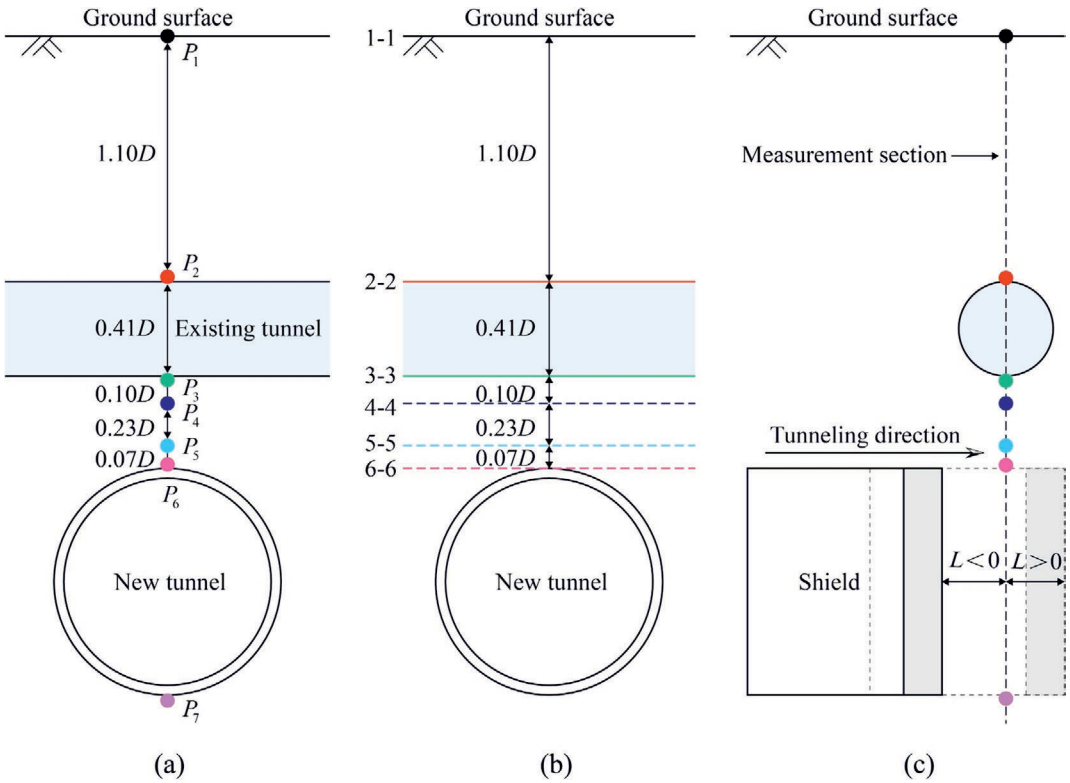

Fig. 5. Details of Case group 4. (a) Positions of measurement lines, (b) positions of measurement points, and (c) definition of L.

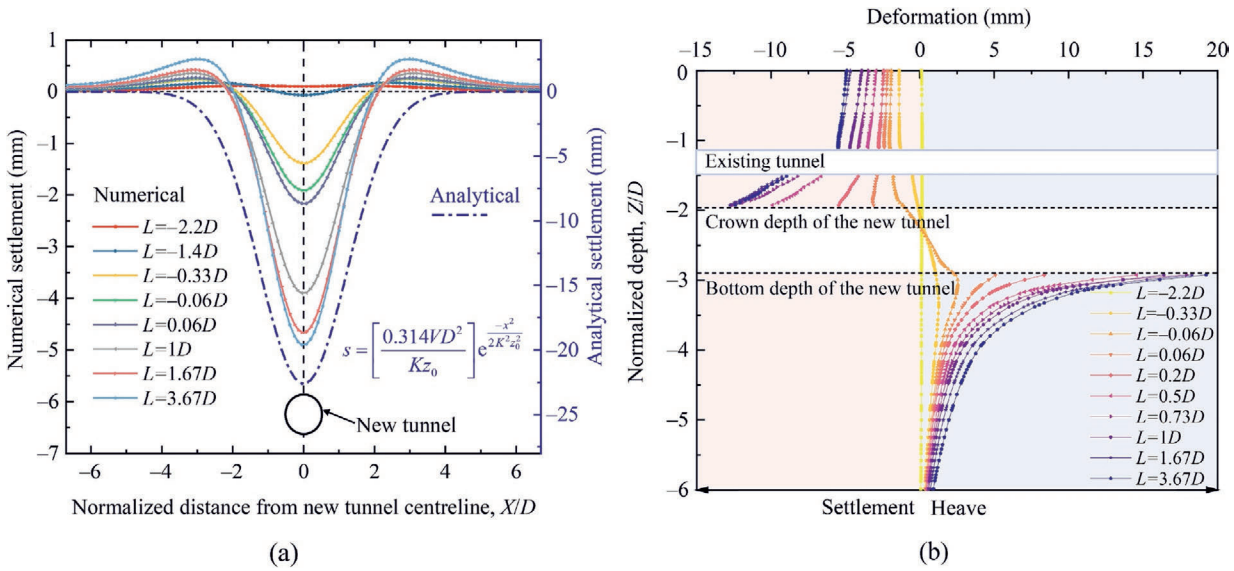

Fig. 6. Deformation of the ground surface and strata during tunneling. (a) Comparison of ground surface settlement troughs along the measurement section obtained from numerical simulation and the Peck formula, and (b) strata deformation with depth along the tunnel centerline.

thermore, parametric studies were performed using 28 numerical models to examine the influences of tunnel spacing and volume loss ratio on strata response and surface deformation.

4.1 Variations of deformations at the measurement section

Figure 6(a) illustrates the variations in the ground surface settlement trough of the measurement section during shield tunneling. At $L = -2.2D$, a minor overall heave of the ground surface marks the onset of tunneling-induced impact. Beyond $L = -1.4D$, heave is observed primarily at trough shoulders, gradually increasing as the shield advances but remaining below 1 mm. The maximum settlement, occurring at the tunnel centerline, exhibits the most significant variation as the tunnel face passes the measurement section, reaching approximately half of the final settlement. Beyond $L = 3.67D$, the settlement trough stabilizes. The Peck empirical formula, widely used for predicting tunneling-induced surface deformation, is presented in a format conducive to engineering applications, as shown in Eq. (1) (Xie et al., 2016):

$$s = \left[\frac{0.314VD^2}{Kz_0}\right] e^{\frac{-x^2}{2K^2z_0^2}}, \tag{1}$$

where s is the surface settlement at a distance x from the tunnel centerline; V is the volume loss ratio; D is the outer diameter of the new tunnel; K is the trough width parameter (set to 0.5 for Shanghai strata); and z_0 is the tunnel axis depth. Figure 6(a) compares the numerical simulation results with the Peck formula, revealing that the latter predicts larger settlements. This discrepancy arises because the Peck formula neglects the stiffness of the existing tunnel. However, the existing tunnel behaves as a rigid stratum

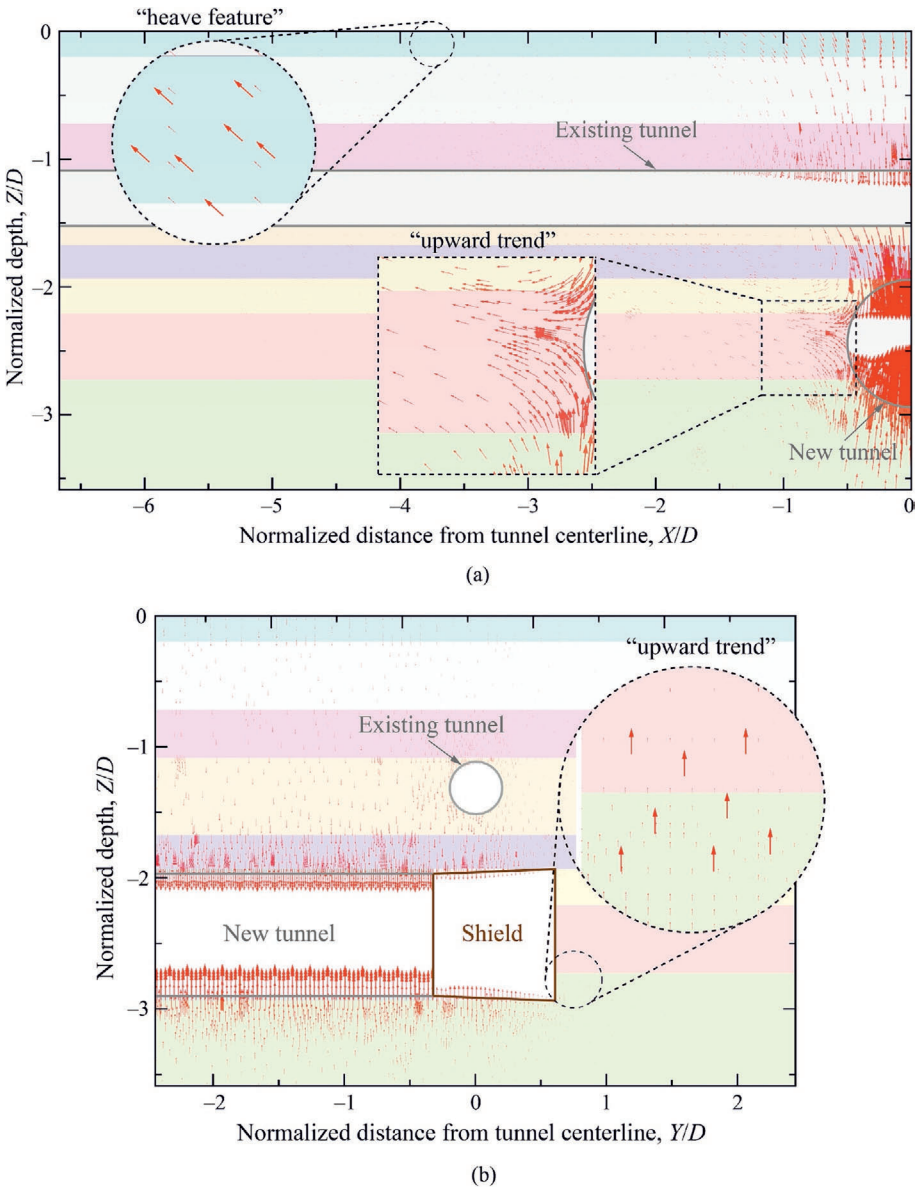

Fig. 7. Ground displacement $|u|$. (a) Transversal section, and (b) longitudinal section.

with equivalent bending stiffness, restricting the upward spread of strata deformation (Zhou et al., 2020). Consequently, the Peck formula tends to overestimate settlement near existing tunnels.

Figure 6(b) shows strata deformation with depth at the tunnel centerline during shield tunneling. The soil above the existing tunnel settles uniformly, while the soil sandwiched between the existing and new tunnels ($-1.92 < Z/D < 1.51$) experiences a sharp increase in settlement with depth, potentially causing vertical elongation of the existing tunnel. Near the crown of the new tunnel, excessive settlement may cause soil detachment from the overlying layers, while the soil beneath the new tunnel undergoes heave-type deformation due to unloading. Overall, as the tunnel face progresses along the tunnel centerline, the soil above the new tunnel settles, while the soil below it heaves. Figure 7(a) illustrates ground displacement in the transversal section, denoted as $|u|$, with red arrows indicating soil movement. The soil beneath the new tunnel heaves, driving the soil in the square area upwards. This "upward trend" transmits to the ground surface, contributing to the "heave feature" at the shoulders of the settlement trough. Figure 7 (b) presents the longitudinal plane, illustrating the soil heaving beneath the new tunnel, which induces the "upward trend" in ground displacement, as highlighted in the magnified circular area.

Figure 8 illustrates settlement progression at six measurement points (Fig. 5(a)) during tunneling. At $L = -1D$, noticeable settlement occurs at all points. Points P_3, P_4, P_5, and P_6, located between the new and existing tunnels, exhibit increased settlement rates as the tunnel face advances through the measurement section. P_5 and P_6, closer to the new tunnel, show higher settlement rates, indicating potential soil damage and loosening. Figure 9 presents the evolution of settlement troughs along the six measurement lines (Fig. 5(b)) at corresponding depths. At $L = -0.06D$, the settlement at P_1 is the largest, with the widest transverse settlement trough, while the settlement at P_6 is the least (Fig. 9(a)). When the tunnel face crosses the measurement section ($L = 0.06D$), settlements at P_3, P_4, P_5, and P_6 surpass those at P_1 and P_2. At $L = 3.67D$, the settlement trough near the new tunnel is the narrowest and deepest, with the largest settlement observed at P_6.

4.2 Variations of stresses at the measurement section

Figure 10(a) illustrates variations in σ_{zz}-depth curves along the tunnel centerline during tunneling, with σ_{zz} remaining almost constant within $-1.1 < Z/D < 0$. Figure 10(b) magnifies the region between the two tunnels ($-1.92 < Z/D < -1.51$) for detailed analysis, where σ_{zz}-depth curves exhibit two distinct types of inflection points ($\oplus$), labeled as 1 and 2. Based on the variation characteristics of σ_{zz}, five phases can be identified.

Phase 1 ($L \le -2.2D$): σ_{zz} increases linearly with depth, matching the initial earth stress ($\sigma = \gamma Z$), indicating no tunneling influence at the measurement section.

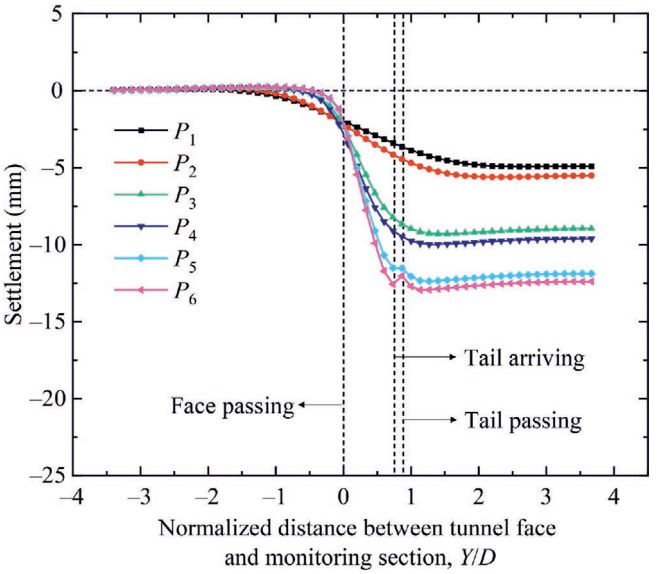

Fig. 8. Settlement progression at the six measurement points during tunneling.

Phase 2 ($-2.2D < L \le -0.06D$): For $-1.92 < Z/D < -1.51$, σ_{zz} exceeds initial earth stress and gradually increases with depth. At $L = -0.06D$, inflection point 2 emerges, below which σ_{zz} grows faster than initial stress, indicating that the soil in this region may be in a compression-tightened state. This phenomenon, also observed by Lin et al. (2019b), is termed as the "compaction zone" in this study.

Phase 3 ($-0.06D < L \le 0.73D$): For $-1.92 < Z/D < -1.51$, σ_{zz} falls below initial stress. At $L = 0.06D$, inflection point 1 emerges, serving as a key indicator for identifying soil arching development and distinguishing the loosened and soil arching zones (Chen et al., 2011; Lin et al., 2019b; Song et al., 2023). Due to the influence of the existing tunnel, the soil above point 1 does not fully develop into a complete soil arching zone and is thus termed as the incomplete soil arching (ISA) zone. The sharp decrease in σ_{zz} between points 1 and 2 defines the loosened zone, corresponding to the increased settlement rates of P_5 and P_6 observed as the tunnel face advances through the measurement section (Section 4.1). As tunneling progresses, point 1 rises, indicating the upward movement of the loosened zone. At $L = 0.73D$, point 2 disappears.

Phase 4 ($0.73D < L \le 1.67D$): After the shield tail passes through the measurement section, the σ_{zz}-depth curve experiences minor changes. Point 1 shifts slightly, signifying that the height of the loosened zone marginally reduces. At $L = 1.67D$, point 2 reappears.

Phase 5 ($L \ge 1.67D$): The σ_{zz}-depth curves stabilize, indicating no further tunneling influence on the measurement section.

Figure 11 shows three-dimensional stress variations at P_3, P_4, and P_5 during tunneling. As the tunnel face approaches the measurement section, σ_{zz} remains stable at P_3 but increases at P_4 and P_5. When the tunnel face

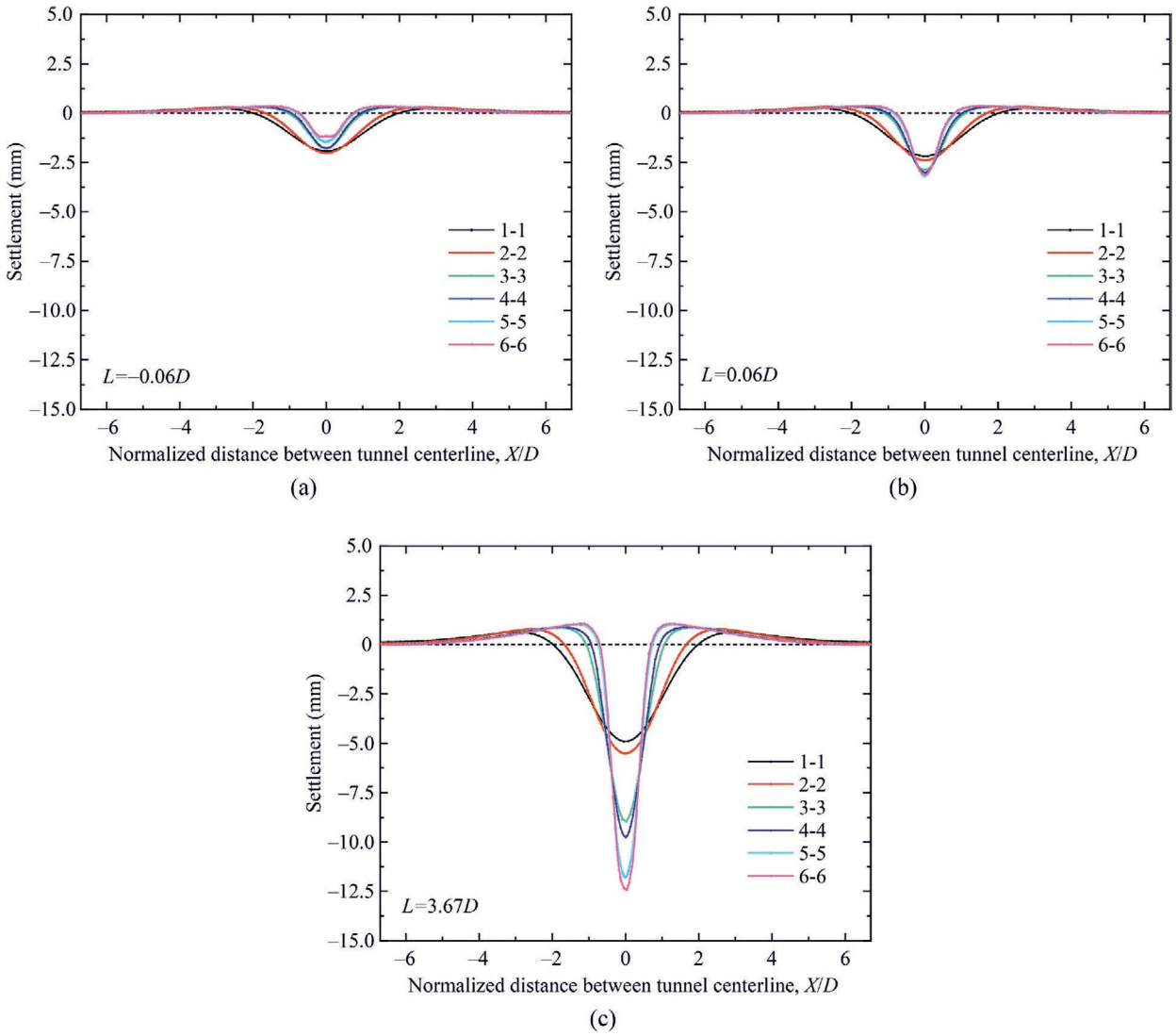

Fig. 9. Evolution of settlement troughs along six measurement lines: (a) $L = -0.06D$, (b) $L = 0.06D$, and (c) $L = 3.67D$.

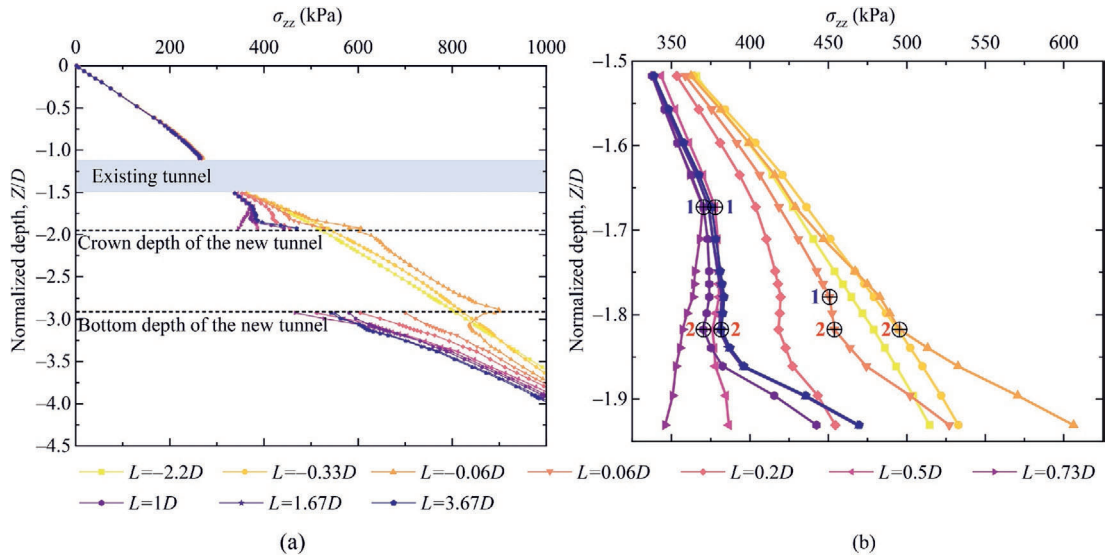

Fig. 10. Variation in σ_{zz} during tunneling. (a) Variation in σ_{zz}-depth curves along the tunnel centerline, with (b) an enlarged view of the region between the two tunnels ($-1.92 \le Z/D \le 1.51$).

passes through the measurement section, σ_{zz} drops sharply at all three points, with the greatest decrease at P_5. Horizontal stresses (σ_{xx}, σ_{yy}) increase at P_3 and P_4, indicating the occurrence of vertical soil arching in the *X*-*Z* and *Y*-*Z* planes (Lin et al., 2019b). However, at P_5, σ_{xx} and σ_{yy} follow a nonmonotonic trend. As the shield tail traverses the measurement section, grouting pressure causes a sudden increase in σ_{zz} at P_5, after which the stresses gradually stabilize. At P_3 and P_4, the increase in σ_{xx} compared with the initial stress is significantly larger than that of σ_{yy}, suggesting stress redistribution mainly through vertical soil arching in the *X*-*Z* plane. At P_5, the three-dimensional stresses fall below initial values, indicating that P_5 is more profoundly affected by the new tunnel, potentially leading to complete destruction and loosening.

This analysis of stress variations reveals the ISA effect and defines three zones: ISA, loosened, and compaction zones. The method for determining these zones will be detailed in the next section.

4.3 Response zone division

Chen et al. (2013) defined the arch foot during tunneling as the region where the horizontal stress concentration ratio ($\lambda_h = \sigma_{hh}/\sigma_{hh,0}$) exceeds 1, while the vertical stress concentration ratio ($\lambda_v = \sigma_{vv}/\sigma_{vv,0}$) is below 1. Here, σ_{hh} and σ_{vv} represent post-tunneling stresses, while $\sigma_{hh,0}$ and $\sigma_{vv,0}$ denote initial stresses. Lee et al. (2006) studied the soil arching effect in soft clay, identifying the upper boundary of the soil arching zone where vertical stress reduces by

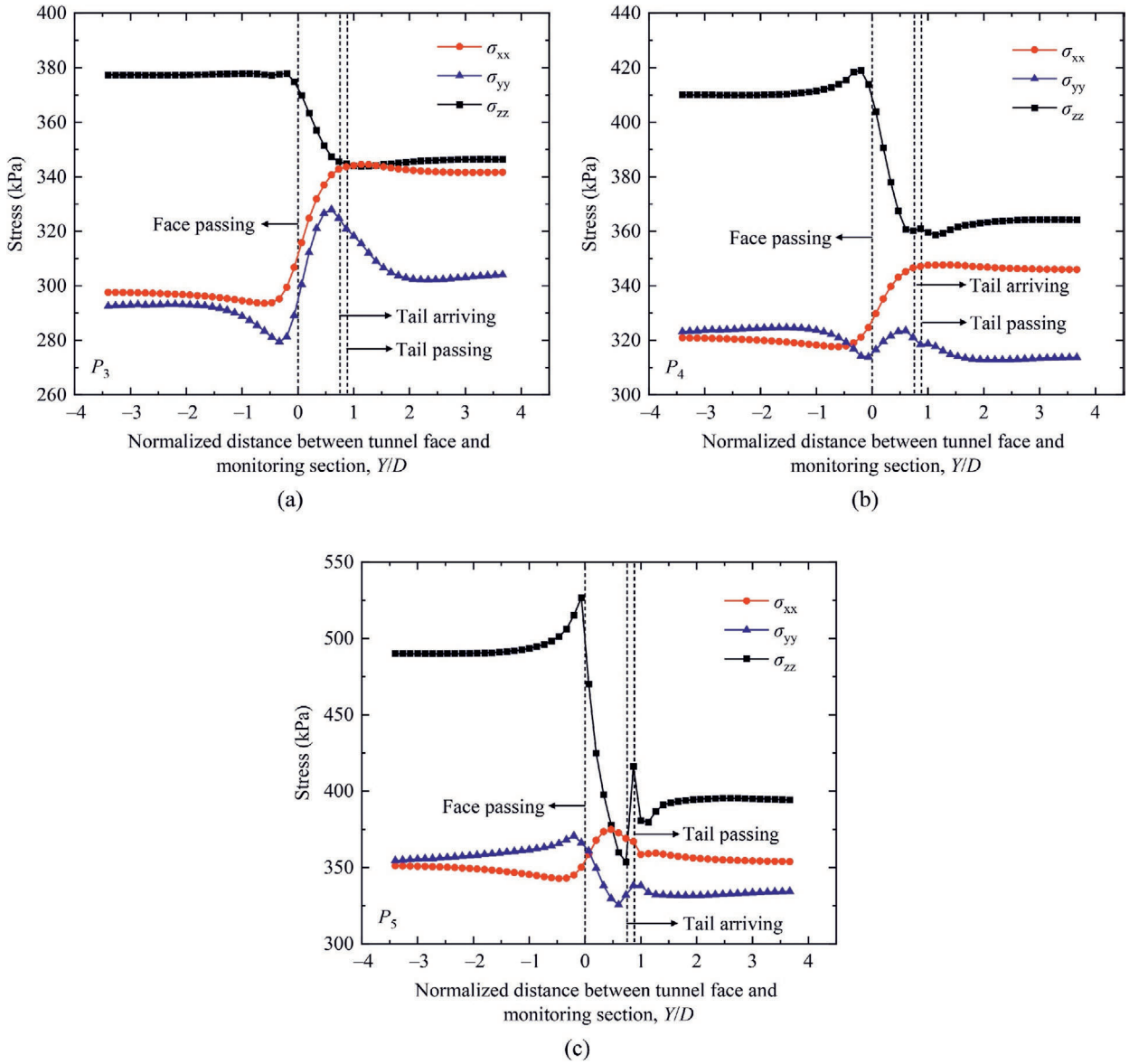

Fig. 11. Variation in three-dimensional stresses at three measurement points during tunneling: (a) P_3, (b) P_4, and (c) P_5.

over 1%, and classifying arching zones as positive or negative based on vertical stress changes: increasing for positive and decreasing for negative.

In this study, abrupt horizontal stress changes at stratigraphic boundaries prompt using vertical stress variations (σ_{zz}) to define the upper, lower, and lateral boundaries of the ISA zone, following Lee's research. Figure 12 shows σ_{zz}-depth curves along vertical measurement lines, where the upper boundary of the ISA zone is marked by a σ_{zz} decrease exceeding 1% (circle points in Fig. 12), and the lower boundary corresponds to inflection points 1 (triangle points). Inflection points 2 (square points) separate the loosened and compaction zones. The lateral boundary is established by the demarcation between positive and negative arching zones, with σ_{zz} increases defining positive zones and decreases indicating negative ones. This study focuses on the ISA zone between the new and existing tunnels ($-1.73 \leq Z/D \leq -1.32$).

4.3.1 Determination of ISA zone, loosened zone, and compaction zone during shield tunneling

Figure 13 shows the ISA, loosened, and compaction zones within the measurement section at different tunneling steps, while Fig. 14 illustrates their evolution. As the tunnel face advances from $L = 0.06D$ to $L = 0.73D$, the loosened zone expands over the compaction zone, extending upward and laterally. Meanwhile, the ISA zone also expands, but cannot form a complete arch due to the existing tunnel. When $L = 0.73D$, the loosened zone reaches its maximum height ($0.26D$), and the compaction zone temporarily disappears due to grouting pressure. By $L = 1D$, the lateral boundary of the ISA zone contracts toward the tunnel centerline, slightly reducing the height of the loosened zone, while the compaction zone reappears. By $L = 3.67D$, both the ISA and loosened zones continue contracting inward.

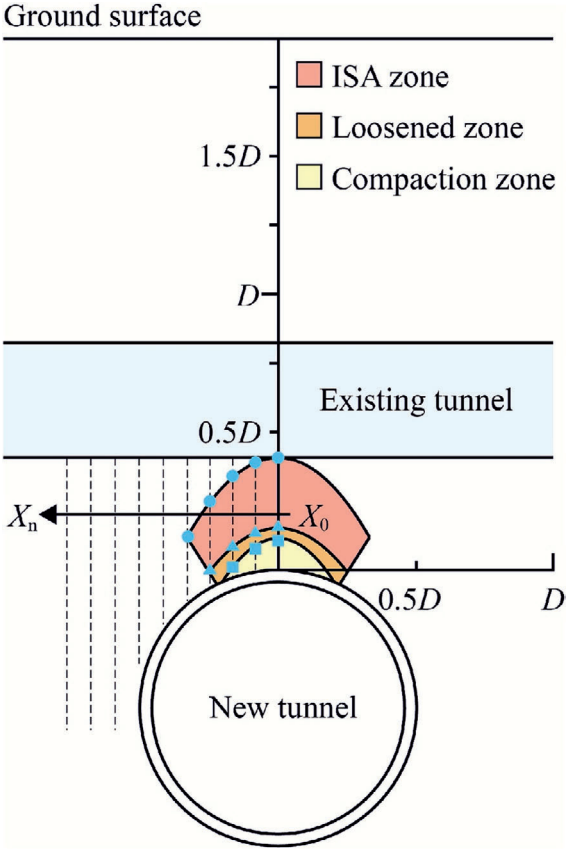

Fig. 12. Schematic illustrating methods for determining the ISA zone, loosened zone, and compaction zone.

4.3.2 Validation of determination methods

Figure 15 presents shear strain distribution and major principal stress trajectories at the measurement section when $L = 1D$. The soil arching effect redistributes stress, transferring earth stress from the negative to the positive arching zone via shear stress. High shear strain regions indicate potential shear surfaces where relative slip may occur (Lin et al., 2019b), defining the boundary between positive and negative arching zones. As shown in Fig. 15 (a), the lateral boundary of the ISA zone aligns closely with the distribution of maximum shear strain.

The major principal stress trajectory defines the soil arching zone (He et al., 2023; Meng et al., 2022). Stress rotation indicates the influence of shield tunneling, with stresses becoming nearly horizontal along the centerline of the soil arching zone, signifying load transfer to both sides. Figure 15(b) shows the upper boundary of the loosened zone, above which major principal stresses along the tunnel centerline become nearly horizontal, confirming their location within the soil arching zone and validating the determined boundaries for the soil arching and loosened zones.

4.3.3 Division of influenced zones in orthogonal undercrossing tunnel engineering

For practical applications, the influence zone of shield tunneling is classified into three areas: reinforced, stable, and safe zones (Fig. 16). The reinforced zone, representing the outermost boundary of the expanded loosened zone, exhibits a significant increase in settlement rate and a marked reduction in σ_{zz}, indicating potential soil failure. To mitigate damage to the existing tunnel from the upward expansion of the loosened zone, soil reinforcement is recommended, extending $0.26D$ above the new tunnel and $0.42D$ laterally from its centerline. The soil arch, with load-bearing capacity, is categorized as a stable zone. The arch foot beyond the lateral boundary of the ISA zone is determined as a safe zone.

4.4 Parametric analyses on ground responses

Parametric analyses using 28 numerical models (Table 3) investigated the impacts of tunnel spacing and volume loss ratio on ground response, providing optimal recommendations for orthogonal undercrossing tunnel engineering.

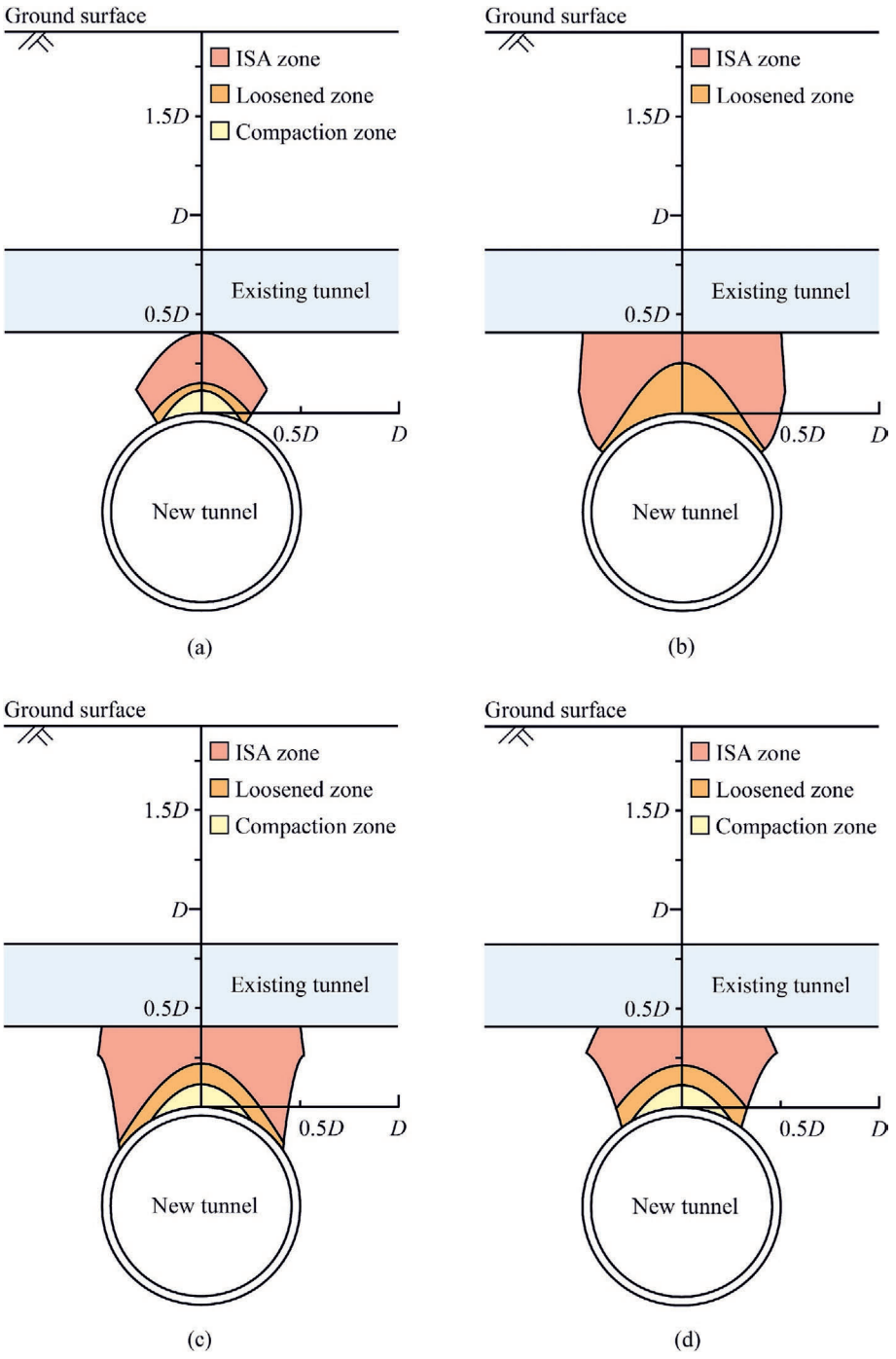

Fig. 13. Spatial distribution of ISA zone, loosened zone, and compaction zone within the measurement section for various representative tunneling steps: (a) $L = 0.06D$; (b) $L = 0.73D$; (c) $L = 1D$; (d) $L = 3.67D$.

4.4.1 Ground deformation

Figure 17 illustrates how tunnel spacing affects settlement troughs at the ground surface for a volume loss ratio of 0.6%. Smaller spacing results in narrower troughs with greater maximum heave and settlement. The maximum settlement significantly increases when $S < 0.3D$.

Figure 18 presents the maximum settlement and heave at the ground surface for various combinations of volume loss ratio and spacing. Smaller volume loss ratios and reduced spacing increase heave, while larger volume loss ratios with reduced spacing intensify settlement. The soil heave is primarily driven by (1) smaller volume loss ratios, which limit earth stress release and increase strata heave, and (2) shallower burial depths for the new tunnel at smaller spacings, amplifying tunneling-induced upward soil movement (Section 4.1). Settlement is influenced by (1) lar-

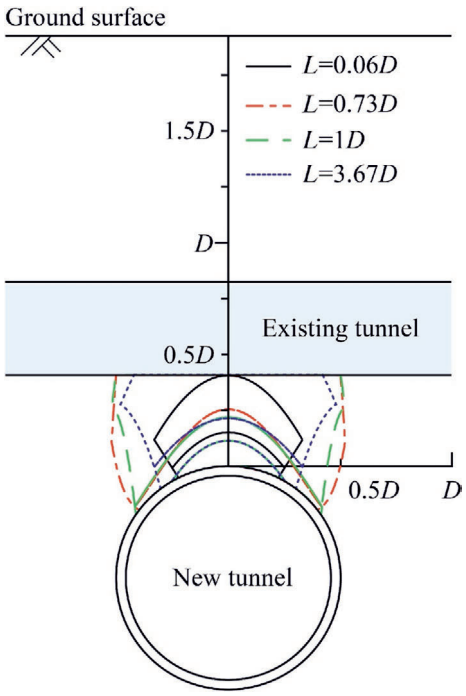

Fig. 14. Evolution of ISA zone, loosened zone, and compaction zone during tunneling.

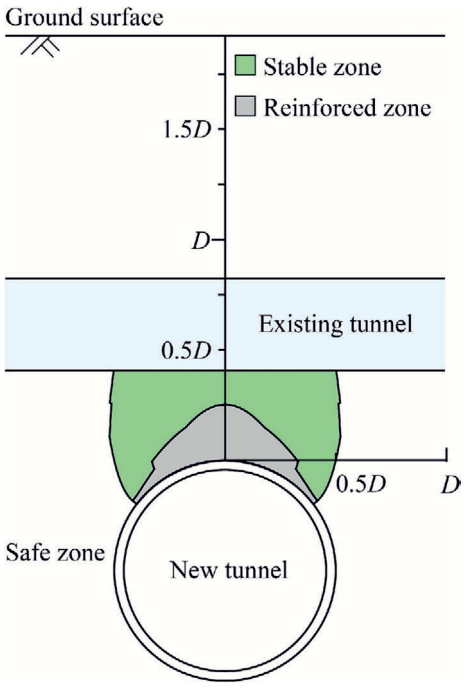

Fig. 16. Influenced zone of shield tunneling in soil.

ger volume loss ratios, enhancing earth stress release and increasing strata settlement, and (2) inadequate formation of a bearing arch at very small spacings, causing significant settlement. The bearing arch refers to the soil arch with a certain bearing capacity, which in this context corresponds to the ISA zone. Deformations of the ground surface follow a consistent pattern across all volume ratios: (1) for $S < 0.3D$, the maximum settlement increases minimally; (2) whereas for $S \geq 0.3D$, the maximum settlement rises significantly; (3) spacing has a greater influence on settlement than heave. For $V = 0.2\%$, settlement is less sensitive to

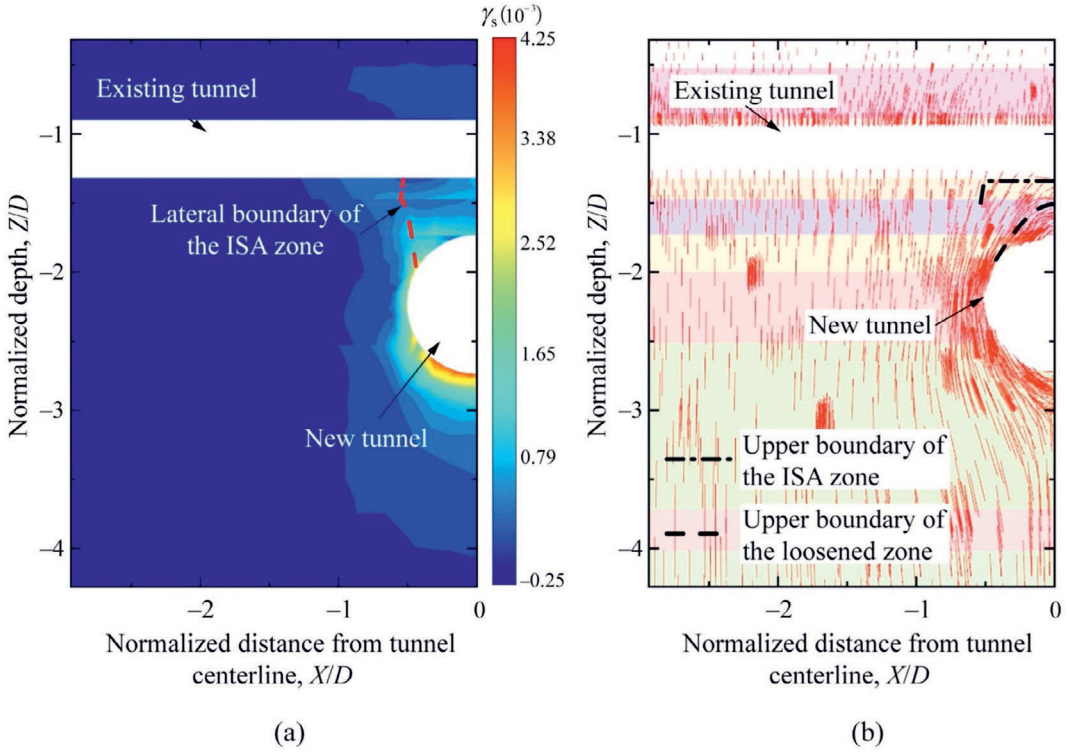

Fig. 15. Soil strain and stress contours at the measurement section. (a) Distribution of shear strain, and (b) trajectory of the major principal stress.

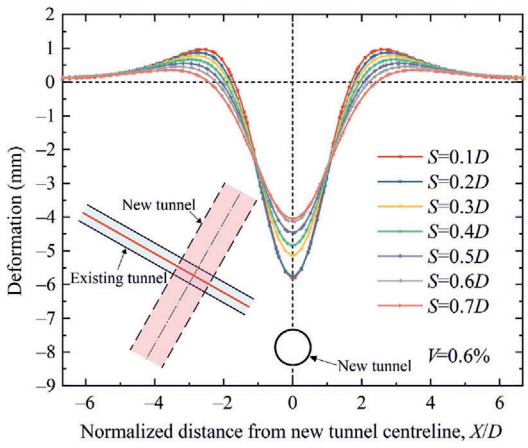

Fig. 17. Settlement troughs at the ground surface in the measurement section.

spacing, suggesting a weaker spacing influence on settlement at lower volume loss ratios (V). Among the seven spacings considered, volume loss ratio affects settlement more than heave, with smaller spacing amplifying its impact.

4.4.2 Height of the loosened zone

Figure 19 shows the maximum deformation values at measurement points and the peak height of the loosened zone (H) during tunneling with a volume loss ratio of 0.6%. Changes in S have little impact on the maximum heave at P_7. When $S \geq 0.3D$, the maximum settlement at P_6 increases as S decreases. No clear pattern is observed in H variations, suggesting S is not the sole influencing factor. When $S < 0.3D$, the maximum settlement at P_6 rises sharply and then stabilizes, with H equating S. This occurs

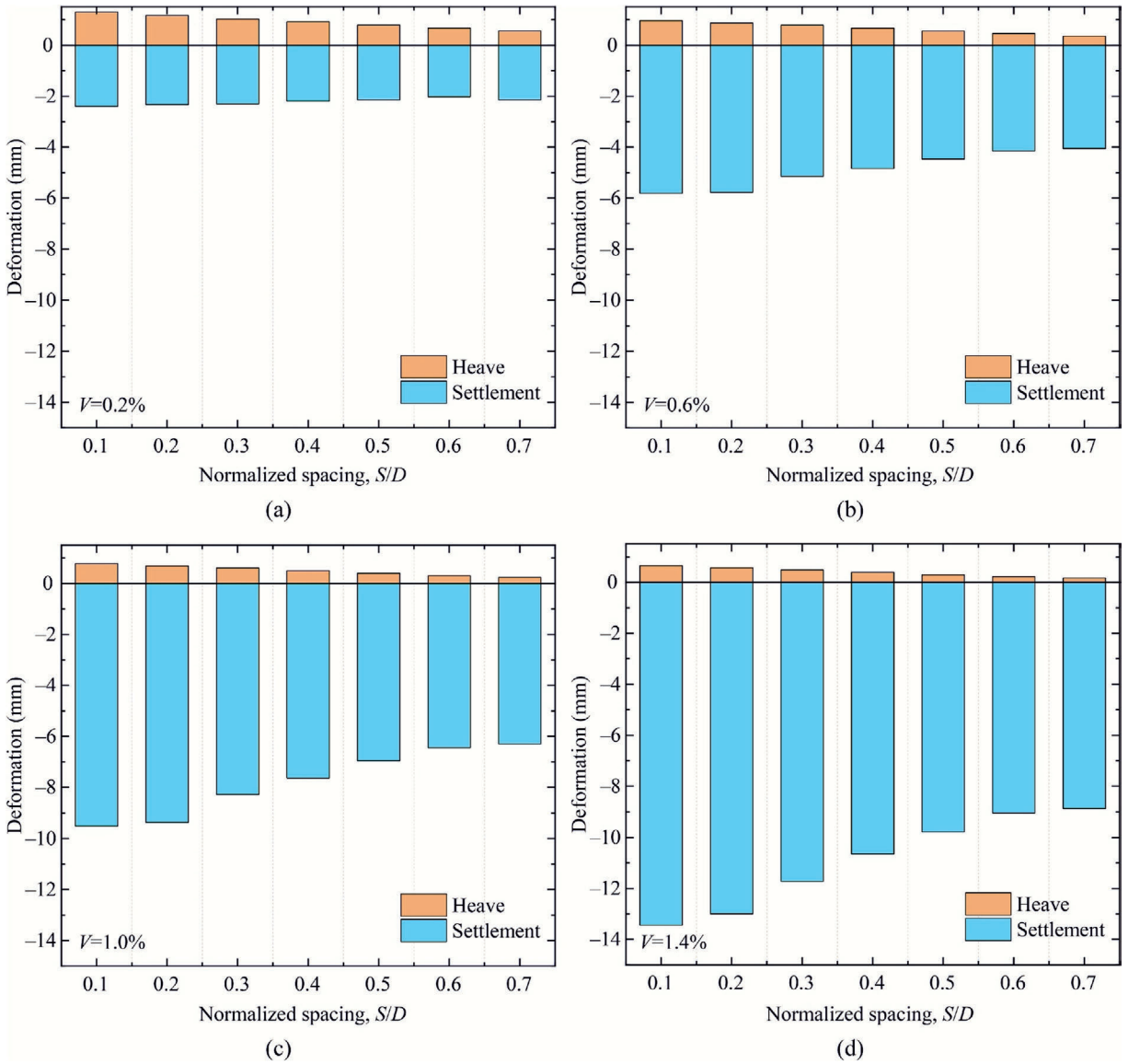

Fig. 18. Maximum settlement and heave values at the ground surface along the measurement section for various combinations of volume loss ratio and spacing: (a) $V = 0.2\%$; (b) $V = 0.6\%$; (c) $V = 1.0\%$; (d) $V = 1.4\%$.

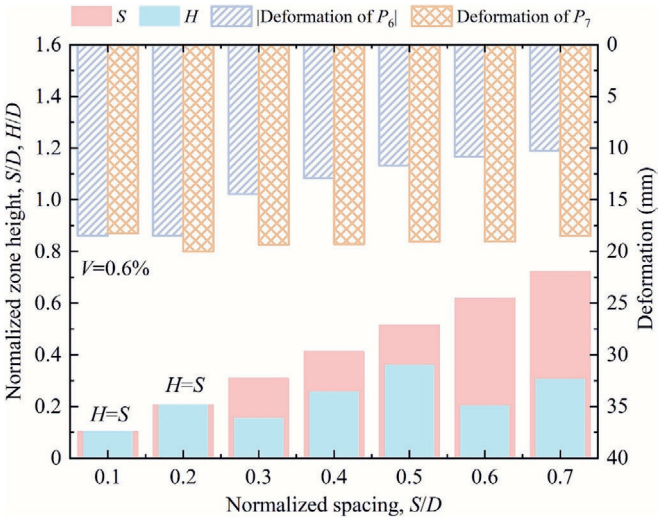

Fig. 19. Maximum deformation at measurement points and peak height of the loosened zone (H).

as the loosened zone's upper boundary reaches the existing tunnel's bottom in cases of excessively small spacing, driving the soil into a limit state (Chen et al., 2013). In this phase, further reductions in S minimally affect the maximum settlement at P_6, suggesting a potential correlation between ground deformation and H/S.

Figure 20(a) presents the peak heights of the loosened zone for various combinations of volume loss ratio and spacing, while Fig. 20(b) shows the ratios of peak height to spacing. When $S < 0.3D$, $H = S$. The above analysis has shown that once the loosened zone reaches the bottom of the existing tunnel, ground and strata deformations increase significantly, rendering $S < 0.3D$ unsafe. When $0.3D \le S \le 0.6D$, inflection point 1 may approach or even rise above the stratigraphic boundary between silty clay ⑤$_1$ and silty clay ⑥ (Fig. 1(b)), strongly was influencing H. In this range, H is affected by two factors: (1) the volume loss ratio (V), and (2) the interaction between inflection point 1 and the stratigraphic boundary separating silty clay ⑤$_1$ and silty clay ⑥.

To enhance the safety of the existing tunnel, it is essential to maintain a greater distance between the loosened zone's upper boundary and the existing tunnel's bottom. Based on our results, a tunnel spacing of no less than $0.3D$ and a volume loss rate not exceeding 0.2% are recommended. This strategy ensures safe tunneling at minimal spacings while guaranteeing adequate separation between the existing tunnel and the loosened zone. The appropriateness of the tunnel spacing and volume loss parameters will be further corroborated by analyzing changes in ground stresses.

4.4.3 Ground stress

Figure 21(a) illustrates the impacts of volume loss ratio and spacing on the incremental vertical stress ($\Delta\sigma_{zz}$), at point P_3, quantified as

$$\Delta\sigma_{zz} = \sigma_{zz} - \sigma_{zz,0}, \quad (2)$$

where σ_{zz} and $\sigma_{zz,0}$ are the post-tunneling and initial vertical stresses, respectively.

For all seven spacings, $\Delta\sigma_{zz}$ decreases as the volume loss ratio increases, with the rate of change in $\Delta\sigma_{zz}$ following two distinct patterns: Type I, characterized by a gradual change (for $S \ge 0.3D$), and Type II, characterized by a rapid change (for $S < 0.3D$). The rapid change in Type II occurs because, in these cases, P_3 lies within the loosened zone, where the soil reaches a limit state and becomes more sensitive to the volume loss ratio. For the four volume loss ratios, $\Delta\sigma_{zz}$ decreases as spacing increases, as larger spacing reduces the disturbance to the soil surrounding the existing tunnel.

Figure 21(b) presents a box plot of $\Delta\sigma_{zz}$ as a function of V, summarizing the distribution of $\Delta\sigma_{zz}$ across different spacings ($S = 0.1D$ to $S = 0.7D$) for each V scenario. When $V = 0.2\%$, $\Delta\sigma_{zz}$ exhibits the least discretization, but for $V > 0.2\%$, variability increases significantly. This suggests that at low volume loss ratios, spacing has minimal impact on $\Delta\sigma_{zz}$, indicating limited soil disturbance around the existing tunnel. Thus, under these conditions, spacing appears to be insensitive to the safety of the existing tunnel.

The analysis of ground stress suggests that maintaining $S \ge 0.3D$ and $V \le 0.2\%$ enhances the safety of existing tunnels during the undercrossing of new super-large-diameter shield tunnels.

5 Deformation behaviors of the existing tunnel

Section 4 established safety thresholds for volume loss ratio and tunnel spacing based on the loosened zone height and ground stress changes. Here, we extend our analysis to examine existing tunnel deformation and validate these thresholds.

5.1 Comparison between ground surface settlement and tunnel settlement

Figure 22 illustrates the settlement development at P_1 (ground surface), T_C (tunnel crown), and T_B (tunnel bottom) during tunneling for Case 4-2. P_1 responds first, while T_B is affected last. As the tunnel face approaches the measurement section, the settlement rates at all three points increase. When $L = -0.6D$, T_B shows the greatest settlement rate. After the shield tail passes, the settlements at these points progressively stabilize. By $L = 1.6D$, T_B reaches its maximum settlement value. However, P_1 achieves its peak $0.8D$ later, indicating a delay in ground surface settlement compared to tunnel settlement.

5.2 Parametric analyses on existing tunnel deformation

Figure 23 illustrates the variation in vertical stress at P_3 and the vertical elongation along section I-I' as spacing increases, with a volume loss ratio of 0.6%. As spacing

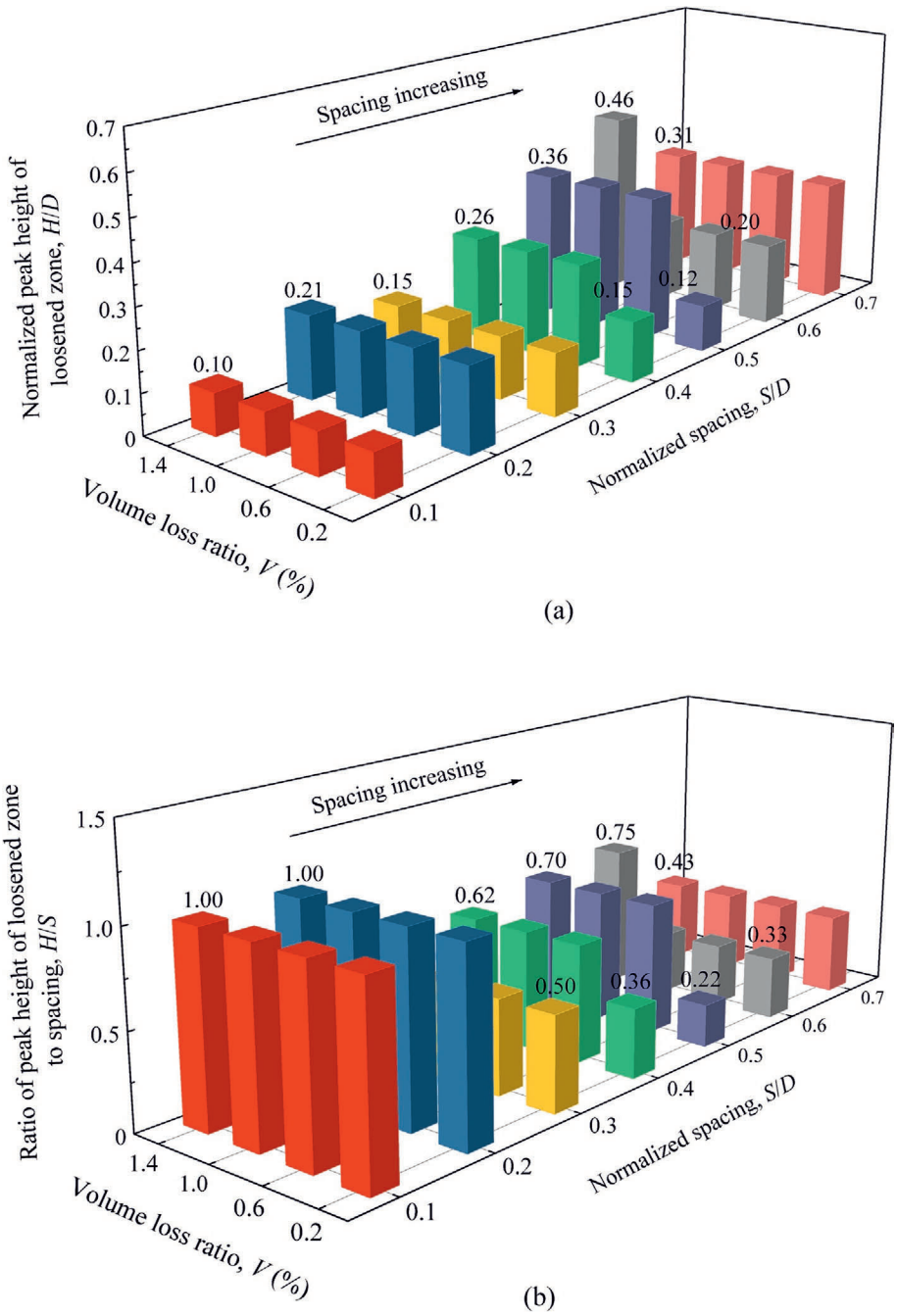

Fig. 20. Parametric effects on the heights of the loosened zone. (a) Peak heights of the loosened zone for various combinations of volume loss ratio and spacing, and (b) ratios of peak heights of the loosened zone to the corresponding spacing.

increases, vertical stress increases while vertical elongation decreases. These trends follow two phases: Phase I ($S < 0.3D$) with rapid changes and Phase II ($S \geq 0.3D$) with gradual changes. In Phase I, the tunnel bottom lies in the loosened zone, resulting in significant ground stress release, causing sharp increases in tunnel deformation, potentially leading to concrete cracking. Moreover, tunnel-soil interaction plays a crucial role, as the existing tunnel alters the distribution of response zones (see Section 4.3), which in turn affects its deformation.

Tunnel convergence, a critical deformation indicator, is widely monitored in engineering. Chinese and British tunnel standards adopt normalized convergence as a structural performance indicator (Huang & Zhang, 2016), defined as

$$C = \Delta D/D. \tag{3}$$

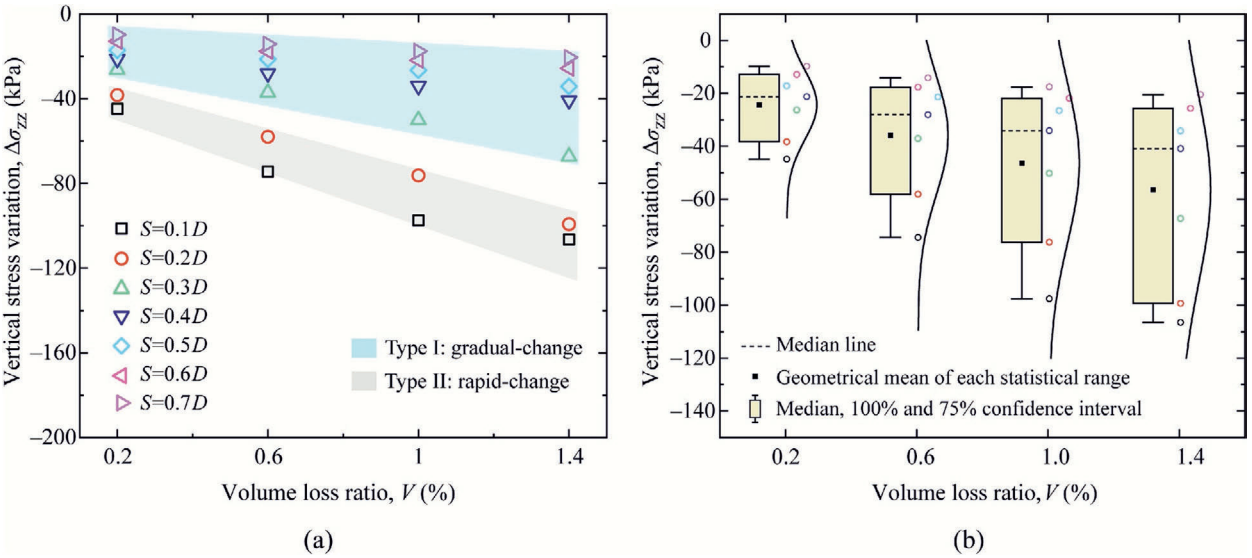

Fig. 21. Parametric effects on $\Delta\sigma_{zz}$. (a) $\Delta\sigma_{zz}$ at P_3 for various combinations of volume loss ratio and spacing, and (b) box plot of $\Delta\sigma_{zz}$.

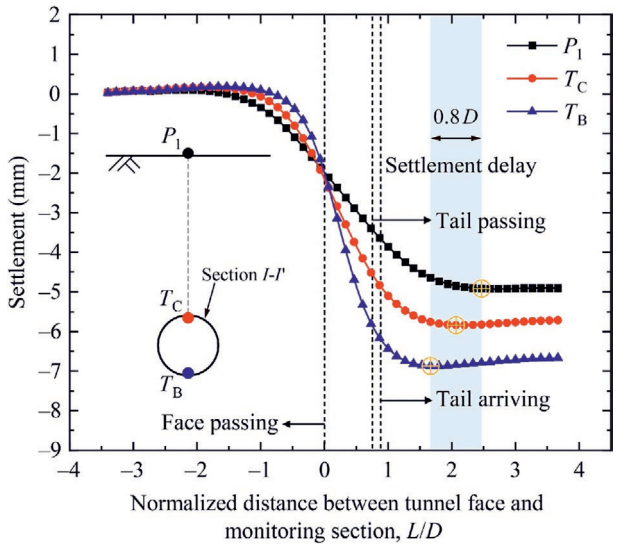

Fig. 22. Development of settlement at P_1, T_C, and T_B of the existing tunnel during tunneling for Case 4-2.

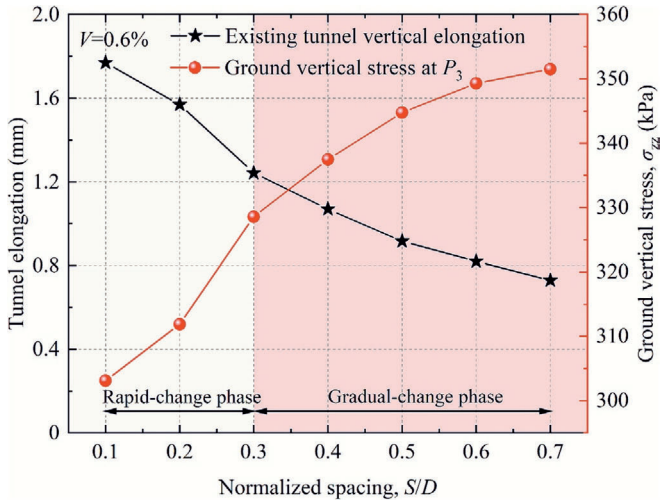

Fig. 23. Variation in vertical stress σ_{zz} at P_3 and vertical elongation of the existing tunnel.

Figure 24 shows the impact of spacing and volume loss ratio on the normalized convergence (C) of the existing tunnel. For each volume loss ratio, C exhibits a two-phase variation, similar to those shown in Fig. 23, depending on whether the tunnel bottom lies in the loosened zone. Reducing spacing from 0.7D to 0.1D increases C by 92.4%, 142.7%, 147.5%, and 135.8% for V = 0.2%, 0.6%, 1.0%, and 1.4%, respectively. The impact of spacing on C is minimal at V = 0.2%, keeping C consistently low. Consequently, when $S \geq 0.3D$ and $V \leq 0.2\%$, tunnel deformation remains low and stable.

In conclusion, to prevent excessive deformation when super-large-diameter shields intersect orthogonally with existing tunnels, the volume loss ratio should not exceed 0.2%, and tunnel spacing should be at least 0.3D, ensuring existing tunnels remain outside the loosened zone, as supported by the findings from Sections 4.4.2 and 4.4.3.

5.3 Protection methods for existing tunnels

Compensation grouting is commonly used to mitigate deformations in existing tunnels and surrounding strata during tunneling by offsetting volume loss (Liu et al., 2024; Wang & Zheng, 2024; Zheng et al., 2022). Although grouting pressure and volume have been extensively studied, research on the grouting area remains limited.

This study reveals that soil in the loosened zone loses bearing capacity, leading to potential structural deformation if the existing tunnel bottom lies within this zone. Therefore, reinforcement is essential to mitigate potential damage (Lin et al., 2019b; Meng et al., 2022). Based on

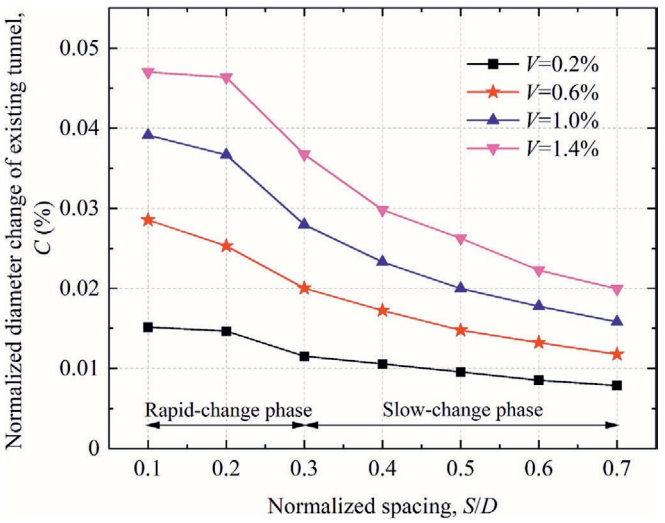

Fig. 24. Normalized convergence of the existing tunnel for various combinations of volume loss ratio and spacing.

our findings, a reinforcement method is proposed: grouting the reinforced zone (Fig. 16) from the new tunnel to improve the mechanical properties of the soil in the loosened zone and control tunnel deformation. Grouting protection is more efficient for small-spacing tunneling than other methods. Moreover, grouting from the new tunnel avoids disrupting the operation of the existing tunnel. Recommended grouting heights, corresponding to the loosened zone heights, are presented in Fig. 20(a) for various spacings and volume loss ratios.

6 Conclusions

In this study, we investigated the impact of shield tunneling on soft ground and adjacent existing tunnels using numerical simulations based on the stratigraphy of Shanghai. We focused on the responses of stress and displacement fields in the strata during the undercrossing of an existing tunnel by a super-large-diameter shield tunnel. The main findings include:

(1) The ISA effect is identified, indicating that the formation of a complete soil arch is hindered by the presence of the existing tunnel.
(2) Methods for defining the ISA, loosened, and compaction zone are proposed, utilizing vertical stress (σ_{zz}) changes and inflection points to delineate boundaries.
(3) Parametric analysis reveals that loosened zone height is affected by the volume loss ratio and tunnel spacing, recommending a volume loss ratio of 0.2% and a minimum spacing of 0.3D as safety thresholds for undercrossing excavations.
(4) The influenced zone is categorized into reinforced, stable, and safe zones, and a grouting strategy is proposed to ensure structural stability without disrupting the operation of the existing tunnel.

Our findings provide practical insights for tunneling design and construction, with further research aimed at addressing different soil types and tunnel configurations.

Data availability

The data that support the findings of this study are available from the corresponding author upon reasonable request.

CRediT authorship contribution statement

Yuyang Cao: Writing – original draft, Conceptualization, Methodology, Data curation, Investigation. **Xiongyao Xie:** Project administration, Methodology, Writing – review & editing, Supervision, Conceptualization, Funding acquisition. **Kun Zeng:** Writing – review & editing. **Yangbin Zhang:** Data curation, Software. **Haiyang Tian:** Supervision, Data curation. **Jian Yao:** Project administration. **Junliang Zong:** Data curation.

Declaration of competing interest

The authors declare that they have no known competing financial interests or personal relationships that could have appeared to influence the work reported in this paper.

Acknowledgement

This work was supported by the National Key R&D Program of China (Grant No. 2023YFC3806705), the National Natural Science Foundation of China (Grant Nos. 52038008 and 52378408), and the Science and Technology Innovation Plan of Shanghai Science and Technology Commission (Grant No. 22dz1203004). Thank you to Mr. Wei Lin for his invaluable guidance on modeling and writing.

References

Avgerinos, V., Potts, D. M., & Standing, J. R. (2017). Numerical investigation of the effects of tunnelling on existing tunnels. *Géotechnique, 67*(9), 808–822.
Benz, T. (2006). *Small-strain stiffness of soils and its numerical consequences*. University of Stuttgart (Germany) (Ph.D. thesis).
Chen, C. N., Huang, W. Y., & Tseng, C. T. (2011). Stress redistribution and ground arch development during tunneling. *Tunnelling and Underground Space Technology, 26*(1), 228–235.
Chen, R. P., Li, J., Kong, L. G., & Tang, L. J. (2013). Experimental study on face instability of shield tunnel in sand. *Tunnelling and Underground Space Technology, 33*, 12–21.
Chen, R. P., Lin, X. T., Kang, X., Zhong, Z. Q., Liu, Y., Zhang, P., & Wu, H. N. (2018). Deformation and stress characteristics of existing twin tunnels induced by close-distance EPBS under-crossing. *Tunnelling and Underground Space Technology, 82*, 468–481.
Chen, R. P., Meng, F. Y., Li, Z. C., Ye, Y. H., & Ye, J. N. (2016). Investigation of response of metro tunnels due to adjacent large excavation and protective measures in soft soils. *Tunnelling and Underground Space Technology, 58*, 224–235.
Cooper, M. L., Chapman, D. N., Rogers, C. D. F., & Chan, A. H. C. (2002). Movements in the piccadilly line tunnels due to the heathrow express construction. *Géotechnique, 52*(4), 243–257.

Ding, Z., Zhang, M. B., Zhang, X., & Wei, X. J. (2023). Theoretical analysis on the deformation of existing tunnel caused by undercrossing of large-diameter slurry shield considering construction factors. *Tunnelling and Underground Space Technology, 133*, 104913.

Do, N. A., Dias, D., Oreste, P., & Djeran-Maigre, I. (2014). Three-dimensional numerical simulation of a mechanized twin tunnels in soft ground. *Tunnelling and Underground Space Technology, 42*, 40–51.

Fang, Q., Liu, X., Zeng, K. H., Zhang, X. D., Zhou, M. Z., & Du, J. M. (2022). Centrifuge modelling of tunnelling below existing twin tunnels with different types of support. *Underground Space, 7*(6), 1125–1138.

Fargnoli, V., Boldini, D., & Amorosi, A. (2013). TBM tunnelling-induced settlements in coarse-grained soils: The case of the new Milan underground line 5. *Tunnelling and Underground Space Technology, 38*, 336–347.

Gan, X. L., Yu, J. L., Gong, X. N., Liu, N. W., & Zheng, D. Z. (2022). Behaviours of existing shield tunnels due to tunnelling underneath considering asymmetric ground settlements. *Underground Space, 7*(5), 882–897.

Guo, X. P., & Jiang, A. N. (2022). Study on the stability of a large-span subway station constructed by combining with the shaft and arch cover method. *Tunnelling and Underground Space Technology, 127*, 104582.

He, J. Z., Liao, S. M., Liu, M. B., Sun, J. C., & Xi, X. G. (2023). The soil arching effect induced by shield tunnelling under asymmetric surface loading. *Computers and Geotechnics, 154*, 105145.

Huang, H. W., Li, Q. T., & Zhang, D. M. (2018). Deep learning based image recognition for crack and leakage defects of metro shield tunnel. *Tunnelling and Underground Space Technology, 77*, 166–176.

Huang, H. W., & Zhang, D. M. (2016). Resilience analysis of shield tunnel lining under extreme surcharge: Characterization and field application. *Tunnelling and Underground Space Technology, 51*, 301–312.

Jin, D. L., Yuan, D. J., Li, X. G., & Zheng, H. T. (2018). An in-tunnel grouting protection method for excavating twin tunnels beneath an existing tunnel. *Tunnelling and Underground Space Technology, 71*, 27–35.

Jin, Y. F., Zhu, B. Q., Yin, Z. Y., & Zhang, D. M. (2019). Three-dimensional numerical analysis of the interaction of two crossing tunnels in soft clay. *Underground Space, 4*(4), 310–327.

Khandouzi, G., & Khosravi, M. H. (2023). An analytical investigation of soil arching induced by tunneling in sandy ground. *Tunnelling and Underground Space Technology, 140*, 105242.

Klar, A., Vorster, T. E. B., Soga, K., & Mair, R. J. (2005). Soil–pipe interaction due to tunnelling: Comparison between Winkler and elastic continuum solutions. *Géotechnique, 55*(6), 461–466.

Lai, H. P., Zheng, H. W., Chen, R., Kang, Z., & Liu, Y. (2020). Settlement behaviors of existing tunnel caused by obliquely under-crossing shield tunneling in close proximity with small intersection angle. *Tunnelling and Underground Space Technology, 97*, 103258.

Lee, C. J., Wu, B. R., Chen, H. T., & Chiang, K. H. (2006). Tunnel stability and arching effects during tunneling in soft clayey soil. *Tunnelling and Underground Space Technology, 21*(2), 119–132.

Li, P., Du, S. J., Ma, X. F., Yin, Z. Y., & Shen, S. L. (2014). Centrifuge investigation into the effect of new shield tunnelling on an existing underlying large-diameter tunnel. *Tunnelling and Underground Space Technology, 42*, 59–66.

Li, X. G., & Yuan, D. J. (2012). Response of a double-decked metro tunnel to shield driving of twin closely under-crossing tunnels. *Tunnelling and Underground Space Technology, 28*, 18–30.

Lin, Q. T., Lu, D. C., Lei, C. M., Tian, Y., Gong, Q. M., & Du, X. L. (2021). Model test study on the stability of cobble strata during shield under-crossing. *Tunnelling and Underground Space Technology, 110*, 103807.

Lin, Q. T., Lu, D. C., Lei, C. M., Tian, Y., Kong, F. C., & Du, X. L. (2022). Mechanical response of existing tunnels for shield under-crossing in cobble strata based on the model test. *Tunnelling and Underground Space Technology, 125*, 104505.

Lin, X. T., Chen, R. P., Wu, H. N., & Cheng, H. Z. (2019a). Deformation behaviors of existing tunnels caused by shield tunneling undercrossing with oblique angle. *Tunnelling and Underground Space Technology, 89*, 78–90.

Lin, X. T., Chen, R. P., Wu, H. N., & Cheng, H. Z. (2019b). Three-dimensional stress-transfer mechanism and soil arching evolution induced by shield tunneling in sandy ground. *Tunnelling and Underground Space Technology, 93*, 103104.

Liu, C., Zhu, D. L., Liu, H., Cui, J., Zhang, X. Y., Rehman, M. U., & Huang, X. Y. (2024). Influence of synchronous grouting on surrounding sandy cobbles during shield tunnelling process: Insights from a scaled model test. *Tunnelling and Underground Space Technology, 147*, 105728.

Liu, X. R., Wang, L. F., Zhou, X. H., Wang, J. M., Zhong, Z. L., Liu, P., Xiong, F., & He, C. (2022). E-M calculation model and its application of calculating deformation in a new tunnel orthogonally undercrossing an existing tunnel. *Tunnelling and Underground Space Technology, 123*, 104418.

Meng, F. Y., Chen, R. P., Xie, S. W., Wu, H. N., Liu, Y., & Lin, X. T. (2022). Excavation-induced arching effect below base level and responses of long-collinear underlying existing tunnel. *Tunnelling and Underground Space Technology, 123*, 104417.

Ng, C. W. W., Boonyarak, T., & Mašín, D. (2015). Effects of pillar depth and shielding on the interaction of crossing multitunnels. *Journal of Geotechnical and Geoenvironmental Engineering, 141*(6), 04015021.

Peck, R. B. (1969). Deep Excavation and tunnelling in soft ground. In *7th International Conference on Soil Mechanics and Foundation Engineering* (pp. 225–290). Mexico.

Qiu, T., Sun, X. H., Chen, X. S., Su, D., Zhang, J. Q., Xu, Z., Song, R., & Wang, X. (2023). Experimental study and resilience modeling for prefabricated hollow diaphragm walls of full-assembled underground stations under urban multi-disturbance conditions. *Tunnelling and Underground Space Technology, 135*, 105044.

Shanghai Shentong Metro Group Co., Ltd., Shanghai Tunnel Engineering & Rail Transit Design and Research Institute, & Tongji Architectural Design (Group) Co., Ltd. (2023). *Technical standard for protection of urban rail transit structures: DG/TJ 08—2434—2023.* Shanghai: Shanghai Municipal Commission of Housing and Urban-Rural Development. (in Chinese).

Soga, K., Laver, R. G., & Li, Z. L. (2017). Long-term tunnel behaviour and ground movements after tunnelling in clayey soils. *Underground Space, 2*(3), 149–167.

Song, X., Wu, H. N., Meng, F. Y., Chen, R. P., & Cheng, H. Z. (2023). Soil arching evolution caused by shield tunneling in deep saturated ground. *Transportation Geotechnics, 40*, 100966.

Wang, L., & Zheng, G. (2024). Numerical analysis of underground displacements stirred by compaction grouting during tunnel construction. *Tunnelling and Underground Space Technology, 152*, 105931.

Wang, W. D., Wang, H. R., & Xu, Z. H. (2013). Study of parameters of HS-Small model used in numerical analysis of excavations in Shanghai area. *Rock and Soil Mechanics, 34*(6), 1766–1774 (in Chinese).

Weng, X. L., Yu, H. F., Niu, H. S., Hu, J. B., Han, W. W., & Huang, X. M. (2022). Interactive effects of crossing tunnel construction on existing tunnel: Three-dimensional centrifugal test and numerical analyses. *Transportation Geotechnics, 35*, 100789.

Wu, C. S., & Zhu, Z. D. (2018). Comparative study on ground loss ratio due to shield tunnel with different diameters. *Chinese Journal of Geotechnical Engineering, 40*(12), 2257–2265 (in Chinese).

Wu, H. N., Shen, S. L., Chen, R. P., & Zhou, A. N. (2020). Three-dimensional numerical modelling on localised leakage in segmental lining of shield tunnels. *Computers and Geotechnics, 122*, 103549.

Xie, X. Y., Yang, Y. B., & Ji, M. (2016). Analysis of ground surface settlement induced by the construction of a large-diameter shield-driven tunnel in Shanghai, China. *Tunnelling and Underground Space Technology, 51*, 120–132.

Yang, J. L., Liu, C., Chen, Q. S., & Xie, X. Y. (2017). Performance of overlapped shield tunneling through an integrated physical model tests, numerical simulations and real-time field monitoring. *Underground Space, 2*(1), 45–59.

Zheng, G., Su, Y. M., Diao, Y., Zhao, Y. B., Chen, H., & Huang, J. Y. (2022). Field measurements and analysis of real-time capsule grouting to protect existing tunnel adjacent to excavation. *Tunnelling and Underground Space Technology, 122*, 104350.

Zhou, Z., Chen, Y., Liu, Z. Z., & Miao, L. W. (2020). Theoretical prediction model for deformations caused by construction of new tunnels undercrossing existing tunnels based on the equivalent layered method. *Computers and Geotechnics, 123*, 103565.

Zhu, M., Chen, X. S., & Wang, X. T. (2022). Analysis and thinking on structural performance evolution of shield tunnel lining. *Engineering Mechanics, 39*(3), 33–50 (in Chinese).